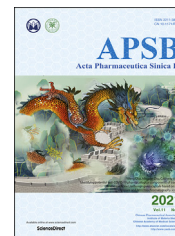




Chinese Pharmaceutical Association  
Institute of Materia Medica, Chinese Academy of Medical Sciences

Acta Pharmaceutica Sinica B

[www.elsevier.com/locate/apsb](http://www.elsevier.com/locate/apsb)  
[www.sciencedirect.com](http://www.sciencedirect.com)



## ORIGINAL ARTICLE

# Discovery of novel diarylamides as orally active diuretics targeting urea transporters



Shun Zhang<sup>a,b,c,†</sup>, Yan Zhao<sup>b,d,e,†</sup>, Shuyuan Wang<sup>b,c</sup>, Min Li<sup>b,c</sup>,  
Yue Xu<sup>b,c</sup>, Jianhua Ran<sup>f</sup>, Xiaoqiang Geng<sup>b</sup>, Jinzhao He<sup>b,c</sup>,  
Jia Meng<sup>b,c</sup>, Guangying Shao<sup>b,c</sup>, Hong Zhou<sup>b,c</sup>, Zemei Ge<sup>b,d</sup>,  
Guangping Chen<sup>g</sup>, Runtao Li<sup>b,d,\*</sup>, Baoxue Yang<sup>a,b,c,\*</sup>

<sup>a</sup>Department of Pharmacology, School of Basic Medical Sciences, Peking University, Beijing 100191, China

<sup>b</sup>State Key Laboratory of Natural and Biomimetic Drugs, Peking University, Beijing 100191, China

<sup>c</sup>Key Laboratory of Molecular Cardiovascular Sciences, Ministry of Education, Beijing 100191, China

<sup>d</sup>School of Pharmaceutical Sciences, Peking University, Beijing 100191, China

<sup>e</sup>College of Pharmacy, Inner Mongolia Medical University, Hohhot 010110, China

<sup>f</sup>Department of Anatomy and Neuroscience Center, Chongqing Medical University, Chongqing 400016, China

<sup>g</sup>Department of Physiology, Emory University School of Medicine, Atlanta, GA 30322, USA

Received 26 March 2020; received in revised form 14 May 2020; accepted 26 May 2020

## KEYWORDS

Urea transporter inhibitor;  
Diuretic;  
Structure optimization;  
Oral administration

**Abstract** Urea transporters (UT) play a vital role in the mechanism of urine concentration and are recognized as novel targets for the development of salt-sparing diuretics. Thus, UT inhibitors are promising for development as novel diuretics. In the present study, a novel UT inhibitor with a diarylamide scaffold was discovered by high-throughput screening. Optimization of the inhibitor led to the identification of a promising preclinical candidate, *N*-[4-(acetylamino)phenyl]-5-nitrofuran-2-carboxamide (**1H**), with excellent *in vitro* UT inhibitory activity at the submicromolar level. The half maximal inhibitory concentrations of **1H** against UT-B in mouse, rat, and human erythrocyte were 1.60, 0.64, and 0.13  $\mu\text{mol/L}$ , respectively. Further investigation suggested that 8  $\mu\text{mol/L}$  **1H** more powerfully inhibited UT-A1 at a rate of 86.8% than UT-B at a rate of 73.9% in MDCK cell models. Most interestingly, we found for the first time that oral administration of **1H** at a dose of 100 mg/kg showed superior diuretic

**Abbreviations:** AQP1, aquaporin 1; BCRP, breast cancer resistance protein; CCK-8, cell counting kit-8; CMC-Na, carboxymethylcellulose sodium; DMF, *N,N*-dimethylformamide; Fa, fraction absorbance; GFR, glomerular filtration rate; HDL-C and LDL-C, high- and low-density lipoprotein; IC<sub>50</sub>, half maximal inhibitory concentration; IMCD, inner medulla collecting duct; *P*<sub>app</sub>, apparent permeability; PBS, phosphate buffered saline; P-gp, P-glycoprotein; r.t., room temperature; THF, tetrahydrofuran; UT, urea transporter.

\*Corresponding authors. Tel./fax: +86 10 82805954 (Runtao Li), +86 10 82805622 (Baoxue Yang)

E-mail addresses: [lirt@bjmu.edu.cn](mailto:lirt@bjmu.edu.cn) (Runtao Li), [baoxue@bjmu.edu.cn](mailto:baoxue@bjmu.edu.cn) (Baoxue Yang).

<sup>†</sup>These authors made equal contributions to this work.

Peer review under responsibility of Institute of Materia Medica, Chinese Academy of Medical Sciences and Chinese Pharmaceutical Association.

<https://doi.org/10.1016/j.apsb.2020.06.001>

2211-3835 © 2021 Chinese Pharmaceutical Association and Institute of Materia Medica, Chinese Academy of Medical Sciences. Production and hosting by Elsevier B.V. This is an open access article under the CC BY-NC-ND license (<http://creativecommons.org/licenses/by-nc-nd/4.0/>).

effect *in vivo* without causing electrolyte imbalance in rats. Additionally, **1H** did not exhibit apparent toxicity *in vivo* and *in vitro*, and possessed favorable pharmacokinetic characteristics. **1H** shows promise as a novel diuretic to treat hyponatremia accompanied with volume expansion and may cause few side effects.

© 2021 Chinese Pharmaceutical Association and Institute of Materia Medica, Chinese Academy of Medical Sciences. Production and hosting by Elsevier B.V. This is an open access article under the CC BY-NC-ND license (<http://creativecommons.org/licenses/by-nc-nd/4.0/>).

## 1. Introduction

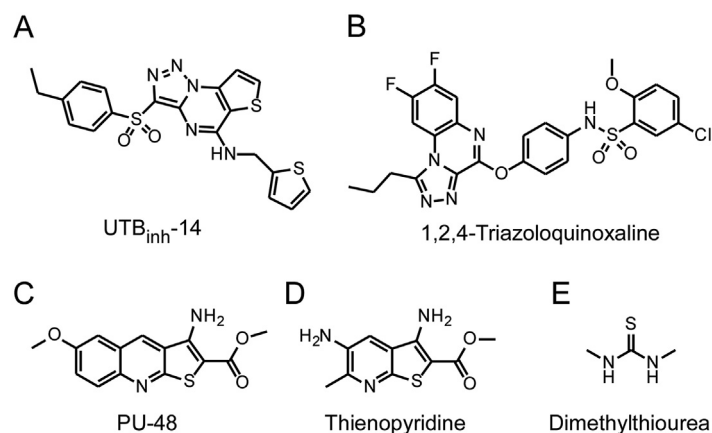
Diuretics are mainly used for the treatment of edema, heart failure, liver cirrhosis, hypertension, and nephrotic syndrome. Common diuretics, such as loop diuretics, thiazide diuretics, potassium-sparing diuretics, and carbonic anhydrase inhibitors, induce diuresis by increasing the excretion of  $\text{Na}^+$ , thus indirectly causing electrolyte disorders, including hypokalemia or hyperkalemia<sup>1–3</sup>, which subsequently increase the risks of arrhythmia and sudden cardiac death.

In addition to electrolytes, urea is also a major solute in the hyperosmolar renal medulla and plays an important role in urinary concentration management<sup>4,5</sup>. Urea transporters (UT), a kind of urea-selective membrane channel proteins, facilitate intrarenal urea recycling<sup>5–9</sup>. UTs include seven isoforms, 6 UT-As (UT-A1–A6), and a UT-B encoded by genes *Slc14a2* and *Slc14a1*<sup>10–12</sup>. In human kidney, UT-A1 and UT-A3 are expressed in the principle cells of the inner medullary collecting duct (IMCD), while UT-A2 is expressed in the thin descending limb. UT-B is expressed in the endotheliocyte of the descending vasa recta in the kidney and other tissues, including erythrocyte, brain, heart, colon, testis, bladder, etc<sup>13</sup>. UTs play a critical role in the generation of concentrated urine<sup>14,15</sup>. The functional inhibition of UTs causes diuresis with relative salt-sparing<sup>13,16–20</sup>. Therefore, as potential diuretic therapeutics, UT inhibitors would not disturb the balance of electrolyte metabolism *in vivo* and can be more suitable for long-term therapy<sup>21–24</sup>. UT-A1 null mice showed higher urine output and fewer extrarenal phenotypes than UT-B null mice, which suggests that UT-A1 is a better diuretic target than UT-B<sup>4</sup>.

In recent decades, several classes of potent small molecule inhibitors of UTs have been identified<sup>25–37</sup>. Among these inhibitors, the triazolothienopyrimidine inhibitor UTB<sub>inh</sub>-14 (Fig. 1A) is the most potent compound targeting UT-B. However, mice showed mild increased urine output and decreased urine osmolality in high vasopressin and fluid-retaining conditions after intraperitoneal administration<sup>26</sup>. Verkman's group<sup>33</sup> reported 1,2,4-triazoloquinoxaline (Fig. 1B) as an UT-A1 inhibitor, which significantly increased the urine output and reduced the urine osmolality after intravenous administration in a rat model.

Our previous work identified a class of UT inhibitors with a thienoquinolin scaffold<sup>31,35,38</sup>, in which PU-48 (Fig. 1C) displayed strong UT inhibition with half maximal inhibitory concentration ( $\text{IC}_{50}$ ) values of 0.32 and 0.22  $\mu\text{mol/L}$  for UT-A1 and -B, respectively<sup>27,28,32</sup>. Moreover, PU-48 exhibited excellent diuretic effect in a rat model after hypodermic injection without influencing the levels of  $\text{Na}^+$ ,  $\text{K}^+$  and  $\text{Cl}^-$  in the blood<sup>38</sup>. Further optimization of PU-48 yielded a thienopyridine UT inhibitor (Fig. 1D) with improved water solubility and activity almost equal to that of PU-48 *in vitro* and *in vivo*<sup>32,37,39,40</sup>. Dimethylthiourea, an urea analogue with millimolar potency for UT inhibition was identified in previous studies (Fig. 1E)<sup>27,30</sup>. Nevertheless, none of the novel UT inhibitors mentioned above was effective *via* oral administration, which significantly prevents their clinical application.

In the present study, we report the discovery of a new structural type of potent UT inhibitor with a diarylamide scaffold. The compound *N*-[4-(acetylamino)phenyl]-4-nitrobenzamide (**E04**) was identified through high-throughput screening of 1040 urea analogues with  $\text{IC}_{50}$  of 5.37  $\mu\text{mol/L}$ . Further optimization of **E04**



**Figure 1** Chemical structures of reported UT inhibitors.

and extensive pharmacodynamic and pharmacokinetic investigation led to the identification of compound **1H** with more potent inhibitory activity for UT-A1 than UT-B. Also noteworthy is that for the first time, **1H** showed highly favorable diuresis after intragastric administration.

## 2. Results and discussion

### 2.1. Discovery of the diarylamide compound **E04** as an UT inhibitor

According to the principles of medicinal chemistry, inhibitors of a certain protein usually have structural characteristics similar to that of its endogenous substrate<sup>41,42</sup>. Thus, urea analogues were considered the most likely small molecules to become UT inhibitors. In fact, some urea analogues with millimolar potency for UT inhibition were identified in previous studies (Fig. 1E)<sup>27,30</sup>. In addition, a crystal structure of UT-B (PDB ID: 6QD5) suggested that both the surface and the pore that permeate urea were largely hydrophobic. The structure of UT-A1 is not clear but should be similar to that of UT-B, so that the UT-B inhibitor can often have a significant inhibitory effect on UT-A1. Due to the lack of an effective experimental model for high-throughput screening of UT-A1 inhibitors, the active compounds for UT-A inhibition can be found from UT-B inhibitors. Based on these considerations, high-throughput screening of 1040 urea analogues containing hydrophobic structural units was conducted using the human erythrocyte lysis model<sup>31</sup>.

Fortunately, three molecules, **A01**, **E04** and **E06** (Fig. 2), with diarylamide scaffolds were found to exhibit UT-B inhibitory activity at a concentration of 10  $\mu\text{mol/L}$  with inhibition rates at 25%, 99%, and 40%, respectively. Further evaluation of the  $\text{IC}_{50}$  showed that **E04** was the most potent compound ( $\text{IC}_{50} = 5.37 \mu\text{mol/L}$ ), which was worth further optimization as a hit compound.

### 2.2. Optimization of **E04**

According to the structure of **E04**, its optimization was divided into three steps (Fig. 3). First, the two aromatic rings ( $\text{Ar}_1$  and  $\text{Ar}_2$ ) were modified to identify the optimal structures. Then, the influence of linker between the two aromatic rings on the inhibition potency was explored. Finally, the substituents on the two aromatic rings ( $\text{R}_1$  and  $\text{R}_2$ ) were optimized.

### 2.3. Optimization of $\text{Ar}_1$ in part A

Keeping part B and the linker of **E04** intact, the benzene ring ( $\text{Ar}_1$ ) in part A was replaced by six- or five-membered heteroaromatic rings, affording compounds **1A–1G**. The inhibitory activities of

these compounds against UT-B are presented in Table 1. It is clear that three compounds (**1C**,  $\text{Ar}_1 = 2\text{-furan}$ ; **1D**,  $\text{Ar}_1 = 2\text{-pyrrole}$ ; **1E**,  $\text{Ar}_1 = 2\text{-oxazole}$ ) exhibited inhibitory activity against human or rat UT-B, and **1C** was slightly better than the others. Additionally, it was observed that removing the nitro group of **E04** led to a total loss in activity (**1A**), which suggested that the nitro group at  $\text{Ar}_1$  was important for the inhibitory activity. Thus, compound **1H** was designed and synthesized by the introduction of the nitro group to the furan ring of **1C**. Compound **1H** showed an  $\text{IC}_{50}$  value of 0.13  $\mu\text{mol/L}$  for human UT-B, which was over 41 and 211 times the activity of **E04** and **1C**, respectively.

### 2.4. Optimization of $\text{Ar}_2$ in part B

On the basis of the results of the optimization of  $\text{Ar}_1$ , we next selected compound **1H** to optimize its  $\text{Ar}_2$  in part B. Various five- and six-membered heterocycles containing one or more heteroatoms were used as part B, affording the compounds **2A–2L**. The activities summarized in Table 2 showed that all compounds exhibited moderate (**2B–2I**) to strong (**2A**) inhibitory activity against UT-B except for the three compounds (**2J–2L**) derived from five-membered heterocycles containing multiple heteroatoms. Among these compounds, compound **2A** ( $\text{Ar}_2 = \text{phenyl}$ ) showed the best activity, which suggested that benzene ring was more favorable than the heterocycles. However, the activity of **2A** was still approximately two times lower than that of compound **1H**. Thus, the effect of the substituents of  $\text{Ar}_2$  on the activity needed further investigation. Moreover, altering the benzene ring to an aliphatic ring (**2M**) led to total loss of activity. This result indicated that the presence of an aromatic structure for  $\text{Ar}_2$  in **1H** is very important for activity.

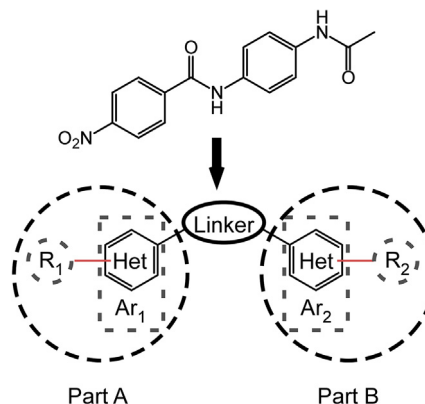


Figure 3 Optimization strategy of the hit **E04**.

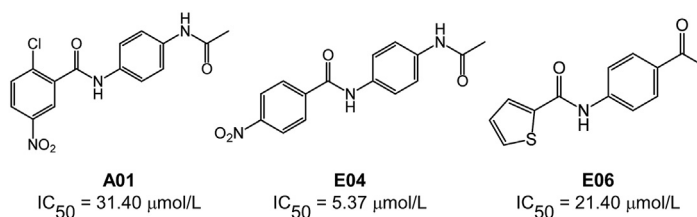
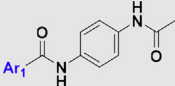


Figure 2 Chemical structures of the hits **A01**, **E04** and **E06** by high-throughput screening.

**Table 1** *In vitro* UT-B inhibition of arylamides with modification of Ar<sub>1</sub>.


Compd.	Ar <sub>1</sub>	IC <sub>50</sub> (μmol/L) <sup>a</sup>		
		Mouse	Rat	Human
<b>E04</b>		>80 <sup>b</sup>	>80	5.37 ± 1.90
<b>1A</b>		>80	>80	>80
<b>1B</b>		>80	>80	>80
<b>1C</b>		>80	>80	27.41 ± 5.60
<b>1D</b>		>80	>80	31.09 ± 10.94
<b>1E</b>		>80	20.62 ± 5.98	>80
<b>1F</b>		>80	>80	>80
<b>1G</b>		>80	>80	>80
<b>1H</b>		1.60 ± 0.32	0.64 ± 0.20	0.13 ± 0.01

<sup>a</sup>IC<sub>50</sub>s are tested with the erythrocyte lysis model. Data are means ± SEM, *n* = 3.

<sup>b</sup>> 80" means the compound shows no activity at concentration of 80 μmol/L.

### 2.5. Optimization of the linker

According to the results of the previous optimization, we selected **1H** as the model to examine the effects of different linkers on the activity. As shown in Table 3, all the changes in the linker, whether inserting methylene between the N atom and aromatic ring (**3A**) or altering the amide to  $\alpha,\beta$ -unsaturated amide (**3B**), imine (**3C**) or amine (**3D**), dramatically reduced potency. Interestingly, replacing the hydrogen on N atom of amide with methyl group (**3E**) led to the loss of activity. Consequently, amide as a linker is essential for UT-B inhibitory activity, and the hydrogen on the N atom should not be replaced.

### 2.6. Optimization of the substituents at aromatic rings

The optimized results above indicated that compound **1H** was a potential UT-B inhibitor. However, considering that nitro compounds easily induce mutagenicity or genotoxicity and substituents on the benzene ring significantly affect activity, we next focused on the optimization of R<sub>1</sub> and R<sub>2</sub>.

For the optimization of R<sub>1</sub>, the 2-nitro group on the furan in **1H** was replaced with various substituents, including methyl (**4A**), bromine (**4B**), acetamino (**4C**), and methylsulfonyl (**4D**). All the changes resulted in a marked decrease in activity (Table 4). Thus, it is necessary to retain the nitro group in the molecule.

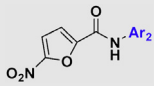
For the optimization of R<sub>2</sub>, to examine the effects of substituted position on activity, moving the 4-acetylamino at the benzene ring in **1H** to the 2- and 3-position given compounds **5A** and **5B**, respectively. It was found that the position of the acetylamino group significantly affected activity. Compared with 4-position substitution (**1H**), 2-substitution (**5A**) caused a significant decrease in the inhibitory activity against the mouse, rat, and human UT-B by 12-, 18-, and 165-fold, respectively. In contrast, the inhibitory activity of 3-substitution (**5B**) on the mouse, rat, and human UT-B increased by 227%, 28%, and 31%, respectively. However, it was disappointed that compound **5B** at a concentration of 15.6 μmol/L showed substantial toxicity to MDCK cells in a cell counting kit-8 (CCK-8) assay, while **1H** did not exhibit significant toxicity to MDCK cells even at a concentration of 62.5 μmol/L (Supporting Information Fig. S1A and B). To verify the toxicity of the 3-substituted analogues, we designed the compound 3-COCH<sub>3</sub> (Fig. S1C), which exhibited significant toxicity to MDCK cells at a concentration of 31.3 μmol/L.

Due to the toxicity profile of 3-substitution (**5B**) and the poor potency of 2-substitution (**5A**), further optimization of R<sub>2</sub> was focused on the 4-substitution. Compounds **5C**–**5K** were designed and synthesized by replacing acetamido with various substituents. As shown in Table 5, substitution with the alkyl group (**5C**, 4-Me) resulted in a total loss in activity. 4-methoxy (**5D**) and 4-hydroxy (**5E**) substitution caused moderate decreases in potency. Halogen-substituted compounds (**5F**, 4-F and **5G**, 4-Cl) and the 4-CN-substituted compound (**5H**) were much less potent than **1H**. Fortunately, compounds **5I** (R<sub>2</sub> = 4-acetyl), **5J** (R<sub>2</sub> = 4-carbomethoxy), and **5K** (R<sub>2</sub> = 4-carbamoyl) with carbonyl groups at R<sub>2</sub> exhibited excellent inhibition activities with IC<sub>50</sub> values of approximately 1 μmol/L. In particular, **5K** showed IC<sub>50</sub> values of 1.58, 0.14, and 0.14 μmol/L for mouse, rat, and human UT-B, respectively, which was similarly potent as **1H** (R<sub>2</sub> = 4-acetylamino). Therefore, the introduction of carbonyl-containing groups was beneficial to activity. Moreover, to improve the solubility, compounds **5L**–**5N** with hydrophilic amines were also designed and synthesized. As expected, these compounds also showed significant activities, especially **5N**, with an IC<sub>50</sub> value of 0.69 μmol/L for human UT-B. However, intragastric administration of **5N** at a dose of 100 mg/kg did not show any diuretic activity on rats.

### 2.7. Chemistry

Most of the target compounds possess a scaffold of amide, which could be constructed using carboxylic acid and amine as building blocks. Synthesis route of compounds **1A**–**1H** and **4A**–**4D** was described in Scheme 1. Substituted or unsubstituted aromatic carboxylic acids **6A**–**6L** were treated with oxalyl chloride under catalysis of *N,N*-dimethylformamide (DMF) in CH<sub>2</sub>Cl<sub>2</sub> to give the corresponding aromatic acyl chlorides **7A**–**7L**, which were subsequently reacted with 4-acetylmino phenylamine (**8**) under basic conditions in tetrahydrofuran (THF) to afford the target compounds **1A**–**1H** and **4A**–**4D**.

The synthesis of substituted furoic acid building blocks **6K** and **6L** was depicted in Scheme 2. The nitro in compound **9** was first reduced into amino (**10**). Then, acetylation of amino and hydrolysis of ester obtained 5-acetylaminofuran-2-carboxylic acid (**6K**). 5-methylsulfonyl furan-2-carboxylic acid (**6L**) was prepared from methyl 5-bromofuran-2-carboxylate (**12**) by methyl sulfonylation and further ester hydrolysis<sup>43</sup>.

**Table 2** *In vitro* UT-B inhibition of compounds **2A–2M**.


Compd.	Ar <sub>2</sub>	IC <sub>50</sub> (μmol/L) <sup>a</sup>		
		Mouse	Rat	Human
<b>1H</b>		1.60 ± 0.32	0.64 ± 0.20	0.13 ± 0.01
<b>2A</b>		3.68 ± 0.39	2.11 ± 0.90	1.30 ± 0.12
<b>2B</b>		5.02 ± 1.84	7.77 ± 1.24	1.96 ± 0.53
<b>2C</b>		7.86 ± 1.29	9.93 ± 1.62	5.28 ± 1.05
<b>2D</b>		3.72 ± 0.37	8.62 ± 2.65	3.17 ± 0.66
<b>2E</b>		38.35 ± 2.56	23.88 ± 9.46	18.38 ± 3.04
<b>2F</b>		9.45 ± 0.09	6.83 ± 0.85	3.87 ± 0.39
<b>2G</b>		20.19 ± 0.70	20.10 ± 4.72	9.94 ± 2.33
<b>2H</b>		12.80 ± 0.66	24.07 ± 6.84	9.05 ± 0.11
<b>2I</b>		18.18 ± 4.19	23.14 ± 2.92	6.49 ± 0.60
<b>2J</b>		>80 <sup>b</sup>	>80	>80
<b>2K</b>		>80	>80	>80
<b>2L</b>		>80	>80	>80
<b>2M</b>		>80	>80	>80

<sup>a</sup>IC<sub>50</sub>s are tested with the erythrocyte lysis model. Data are means ± SEM, *n* = 3.

<sup>b</sup>> 80" means the compound shows no activity at concentration of 80 μmol/L.

Under the basic conditions, reaction of **7H** with different aromatic or aliphatic amines (**14A–14M** and **15A–15N**) yielded the corresponding products **2A–2N** and **5A–5N** (Scheme 3). Most of the amines could smoothly reacted with **7H** at room temperature (r.t.). However, for amines **14B–14G**, the reactions were performed in dichloroethane at 65 °C for overnight, due to their lower reactivity.

The synthesis of **3A–3E** was the same as that of compounds **1** and **2** (Scheme 4). The building block **18** for **3B** was obtained from aldehyde **17** through Knoevenagel reaction, and **19** for **3E** was acquired by Borch reduction using paraformaldehyde and amine **8** as starting materials. The aldehyde **17** condensed with amine **8** to yield imine **3C**, which was transferred to **3D** by reduction with NaBH<sub>4</sub>.

## 2.8. Diuretic activity of **5K** *in vivo*

Based on the optimization results above, we selected **1H** and **5K** for further *in vivo* investigations, as both of these compounds exhibited excellent UT-B inhibition activities and low cell toxicity *in vitro* (Fig. S1A and D). The diuretic activity of **1H** and **5K** in mice and rats was determined using metabolic cages<sup>38</sup>. After intragastric administration of a dose of 100 mg/kg, **5K** did not

show observable diuretic activity in rats (Supporting Information Fig. S2), while **1H** showed significant diuretic activity (diuretic activity of **1H** will be discussed later). According to our experimental results, **5K** showed *in vitro* inhibition activity on UTs, but no diuretic activity *in vivo*. We assume that this phenomenon may be due to the higher predicted log *P* value of **1H** than **5K** (0.99 vs. 0.21 predicted by Qikprop module from Schrödinger), which results in a better intestinal absorption and a higher oral bioavailability of **1H**. Therefore, we further studied the pharmacological characteristics of **1H** (Fig. 4A).

## 2.9. Inhibition activity of **1H** against UT-B

Using erythrocyte lysis assays, the IC<sub>50</sub> of **1H** against UT-B-mediated urea transport was 1.60 μmol/L in mouse, 0.64 μmol/L in rat, and 0.13 μmol/L in human (Fig. 4B and C). The maximum inhibition rates of **1H** among the mouse, rat, and human cells were almost 100%. As a control, erythrocyte from UT-B knockout mice was lysed at approximately 100% due to lack of UT-B in the membrane (Fig. 4B).

To determine the inhibitory efficacy of **1H** against UT-B, the urea permeability in response to a urea gradient was measured by stopped-flow light scattering. The rapid mixing of rat erythrocyte suspension with 500 mmol/L urea solution led to rapid cell shrinking due to water efflux *via* the water channel aquaporin 1 (AQP1), then cell swelling due to urea influx *via* UT-B and water influx *via* AQP1, which changed the light scattering rate. **1H** significantly reduced the urea influx by inhibiting the UT-B function with obvious dose response (Fig. 4D). After incubating erythrocyte in a 500 mmol/L urea solution for 1 h, the erythrocyte was rapidly mixed with isotonic phosphate buffered saline (PBS). It was found that **1H** also dose-dependently inhibited the UT-B-mediated urea efflux (Fig. 4E). However, the inhibitory activity against UT-B disappeared after **1H** was washed out (Fig. 4F), suggesting that the binding of **1H** with UT-B is reversible.

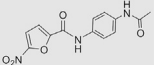
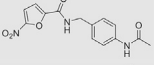
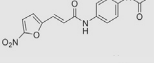
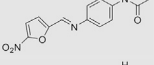
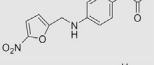
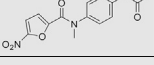
To determine the targeting site of **1H** on the UT-B molecule, the time-dependent UT-B inhibition was measured by stopped-flow light scattering. The inhibitory activity against the inward or outward urea transmembrane transport was significantly time dependent after erythrocyte was incubated with 10 μmol/L **1H** (Fig. 4G and H). Potent inhibition occurred after incubation with **1H** for 5 min, which suggested that **1H** took time to enter the erythrocyte and targeted the intracellular region of UT-B. To further confirm, the putative site of **1H** binding to the UT-B protein was determined by docking computations after homology modeling of the human UT-B structure (accession code, CAB60834) based on crystal structure data of a bacterial UT-B homolog. The predicted binding site was in a pocket of intracellular part of UT-B (Supporting Information Fig. S3A and B). Most of the interactions involved neutral-polar and hydrophobic amino acids, including Phe-301, Phe-176, Phe-71, Leu-364, Leu-121, Thr-368 and so on. We could see that Asn-73 had hydrogen-bonding interactions with oxygen of furan ring and the amide linker, and nitro group built salt bridges with Asp-41 and Lys-43, which proved the structure–activity relationship mentioned above that nitro group of furan and the amide linker is necessary for inhibition effect (Fig. S3C).

## 2.10. Inhibition efficacy of **1H** on UT-B and UT-A1

As UT-B is widely expressed in various tissues, some side effects may occur after inhibition of UT-B. UT-A1 knockout mice



**Table 3** *In vitro* UT-B inhibition of compounds **3A–3E**.

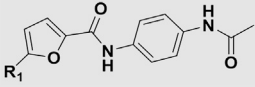
Compd. Structure	IC <sub>50</sub> (μmol/L) <sup>a</sup>		
	Mouse	Rat	Human
<b>1H</b> 	1.60 ± 0.32	0.64 ± 0.20	0.13 ± 0.01
<b>3A</b> 	>80 <sup>b</sup>	>80	>80
<b>3B</b> 	>80	>80	>80
<b>3C</b> 	>80	>80	>80
<b>3D</b> 	>80	>80	>80
<b>3E</b> 	>80	>80	>80

<sup>a</sup>IC<sub>50</sub>s are tested with the erythrocyte lysis model. Data are means ± SEM, *n* = 3.

<sup>b</sup>> 80" means the compound shows no activity at concentration of 80 μmol/L.

showed more powerful diuretic effect than UT-B knockout mice and had no significant extrarenal phenotype<sup>13,19,44–48</sup>. Therefore, it was recognized that UT-A1 is a better diuretic target than UT-B<sup>4</sup>. MDCK cells do not normally express any UTs<sup>36</sup>. The inhibitory activity of **1H** against UT-B and UT-A1 was assayed using MDCK cell lines stably expressing rat UT-B or UT-A1<sup>37</sup>. The rate of 8 μmol/L **1H** inhibition of UT-B-mediated urea transport was 73.9%, while that of UT-A1-mediated urea transport was 86.8% (Fig. 4I–K). The experimental results indicate that **1H** significantly inhibited both UT-A1 and UT-B, and the inhibitory activity against UT-A1 was greater than that against UT-B.

**Table 4** *In vitro* UT-B inhibition of arylamides with modification of R<sub>1</sub>.

Compd. R <sub>1</sub>	IC <sub>50</sub> (μmol/L) <sup>a</sup>		
	Mouse	Rat	Human
<b>1H</b> 	1.60 ± 0.32	0.64 ± 0.20	0.13 ± 0.01
<b>4A</b> CH <sub>3</sub>	>80 <sup>b</sup>	>80	>80
<b>4B</b> Br	15.12 ± 0.30	20.55 ± 1.05	19.73 ± 1.10
<b>4C</b> NHCOCH <sub>3</sub>	16.92 ± 0.48	1.94 ± 0.48	12.98 ± 0.58
<b>4D</b> SO <sub>2</sub> CH <sub>3</sub>	>80	16.13 ± 2.68	13.62 ± 2.07

<sup>a</sup>IC<sub>50</sub>s are tested with the erythrocyte lysis model. Data are means ± SEM, *n* = 3.

<sup>b</sup>> 80" means the compound shows no activity at concentration of 80 μmol/L.

## 2.11. Diuretic activity of **1H** in vivo

**1H** was subcutaneously injected into mice and rats at a dose of 100 mg/kg. Urine was collected every 2 h before and after **1H** administration. Urine output significantly increased in both the mice (Fig. 5A) and rats (Fig. 5B) treated with **1H** compared with the controls. The urine output reached its maximum at the 2nd–4th h after **1H** administration and continued to increase the urine output for the 4th–6th h in mice. The diuretic effect in rats was more effective than that in mice. The urinary osmolality was reduced at the 2nd h after **1H** administration in mice and continued to decrease for 6 h (Fig. 5C). The variation trends of the urine output and urinary osmolality in rats were similar to those in mice (Fig. 5D). The levels of urine output and urinary osmolality returned to the basal level at the 8th–10th h after **1H** administration. The excretion of non-urea solutes was not significantly changed after **1H** administration in both mice and rats (Fig. 5E and F), indicating that **1H** causes diuresis without disturbing the electrolyte metabolism.

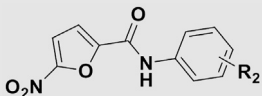
When **1H** (100 mg/kg) was given by gavage, the urine output obviously increased in mice (Fig. 6A) and rats (Fig. 6B) at the 2nd h after **1H** administration. The urinary osmolality decreased in mice (Fig. 6C) and rats (Fig. 6D) at the 2nd–4th h after **1H** administration. The excretion of non-urea solutes in urine was not significantly different between **1H** group and the control group in both mice and rats (Fig. 6E and F), indicating **1H** does not influence electrolyte excretion. The experimental results suggest that **1H** takes effect more quickly by intragastric administration than by subcutaneous administration.

To observe the pharmacological effects of **1H**, mice were treated with 100 mg/kg **1H** every 8 h for 7 days by intragastric administration. **1H** caused continuous diuresis and low urine osmolality (Fig. 7A and B). Meanwhile, daily water intake also increased from 30.0 ± 1.7 to 40.8 ± 4.1 mL (mean ± SEM) after **1H** administration. Unsurprisingly, the excretion of urea and non-urea solutes remained unchanged during long-term **1H** intragastric administration (Fig. 7C and D). It was also confirmed that **1H** could increase the urine output and decrease urinary osmolality (Fig. 7E and F), and the excretion of urea and non-urea solutes remained unchanged during the long-term intragastric administration of **1H** in rats (Fig. 7G and H).

After treatment with 100 mg/kg **1H** every 8 h for 7 days by intragastric administration, the osmolality and solutes in the inner and outer medullary tissues of rats were measured. The results showed that the osmolality and urea concentration were significantly lower in the inner medullary tissue of **1H**-treated rats compared with control-treated rats (Fig. 7I and J). The non-urea solutes exhibited no significant difference between the **1H**-treated rats and control rats (Fig. 7K). However, the osmolality, urea concentration, and non-urea solutes concentration in the outer medulla were not different between the **1H**-treated rats and control rats. These results indicate that **1H** plays a diuretic role by blocking intrarenal urea recycling without interfering with the metabolism of Na<sup>+</sup>, K<sup>+</sup>, and Cl<sup>−</sup>.

## 2.12. Toxicity analysis of **1H**

After 7-day intragastric administration of **1H**, there was no significant difference in body weight and kidney index (ratio of kidney weight to body weight) compared with the control rats (Table 6) or mice (Fig. 8A). Meanwhile, no abnormality was

**Table 5** *In vitro* UT-B inhibition of arylamides with modification of R<sub>2</sub>.


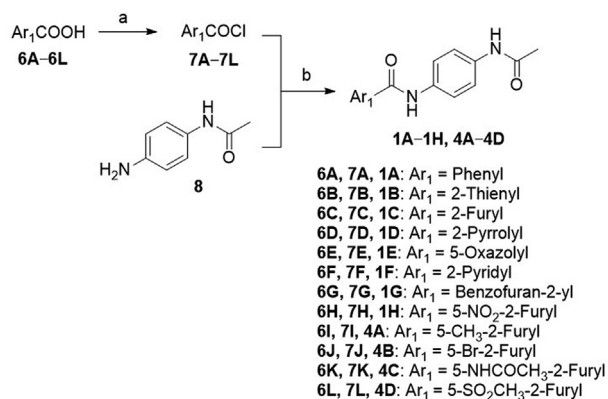
Compd.	R <sub>2</sub>	IC <sub>50</sub> (μmol/L) <sup>a</sup>		
		Mouse	Rat	Human
<b>1H</b>	4-NHCOCH <sub>3</sub>	1.60 ± 0.32	0.64 ± 0.20	0.13 ± 0.01
<b>5A</b>	2-NHCOCH <sub>3</sub>	19.95 ± 0.82	11.68 ± 1.36	21.50 ± 7.65
<b>5B</b>	3-NHCOCH <sub>3</sub>	0.49 ± 0.04	0.50 ± 0.06	0.09 ± 0.01
<b>5C</b>	4-CH <sub>3</sub>	>80 <sup>b</sup>	>80	>80
<b>5D</b>	4-OCH <sub>3</sub>	14.65 ± 2.84	4.20 ± 0.92	2.80 ± 0.74
<b>5E</b>	4-OH	11.27 ± 0.89	3.42 ± 0.45	1.70 ± 0.09
<b>5F</b>	4-F	6.07 ± 0.31	4.22 ± 0.76	4.57 ± 1.22
<b>5G</b>	4-Cl	25.17 ± 3.41	10.43 ± 1.18	25.15 ± 5.64
<b>5H</b>	4-CN	8.88 ± 0.98	1.67 ± 0.38	4.25 ± 0.15
<b>5I</b>	4-COCH <sub>3</sub>	6.66 ± 1.86	1.64 ± 0.14	0.74 ± 0.04
<b>5J</b>	4-COOC <sub>2</sub> H <sub>5</sub>	5.76 ± 0.16	3.02 ± 0.74	1.19 ± 0.06
<b>5K</b>	4-CONH <sub>2</sub>	1.58 ± 0.16	0.14 ± 0.04	0.14 ± 0.01
<b>5L</b>	4-N(CH <sub>3</sub> ) <sub>2</sub>	3.14 ± 0.26	2.28 ± 0.97	5.45 ± 1.33
<b>5M</b>	4-(4-morpholinyl)	11.89 ± 2.61	2.76 ± 0.57	4.06 ± 0.76
<b>5N</b>	4-(4-piperidinyl)	2.94 ± 0.50	0.78 ± 0.28	0.69 ± 0.11

<sup>a</sup>IC<sub>50</sub>s are tested with the erythrocyte lysis model. Data are means ± SEM, *n* = 3.<sup>b</sup>> 80" means the compound shows no activity at concentration of 80 μmol/L.

observed in levels of blood urea and creatinine, suggesting **1H** did not impair renal function (Table 6). No obvious change was occurred in levels of blood Na<sup>+</sup>, K<sup>+</sup> and Cl<sup>-</sup> in rats after **1H** administration, suggesting that **1H** did not influence the electrolyte disturbance that traditional diuretics may lead to (Table 6). Meanwhile, levels of glucose, cholesterol, triglyceride, high-density lipoprotein (HDL-C), and low-density lipoprotein (LDL-C) kept normal after **1H** administration, indicating that **1H** did not influence the glycometabolism, lipid metabolism. HE-staining did not show morphological abnormality in kidney (data not shown).

Glomerular filtration rate (GFR) is the gold standard to assess overall kidney function. We detected whether **1H** influenced GFR on mice and did not find any abnormality after **1H** administration (Fig. 8B).

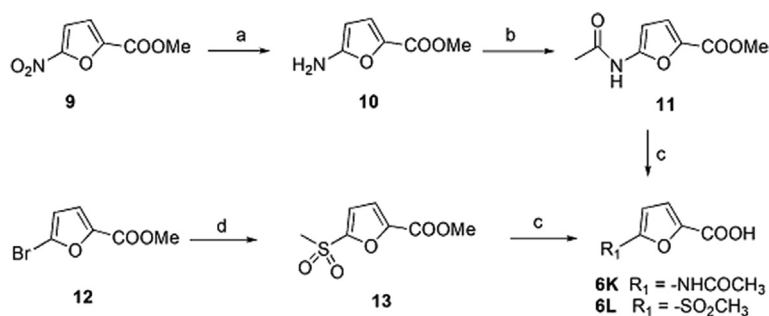
Comparing with common diuretics, **1H** did not change the non-urea solutes excretion in the urine, and not influence the Na<sup>+</sup>, K<sup>+</sup> and Cl<sup>-</sup> in blood, indicating less side effect, such as hypokalemia, hyponatremia, hyperuricemia, caused by common diuretics. Meanwhile, **1H** did not influence normal renal function and glycometabolism, lipid metabolism in the body, suggesting that **1H** is an ideal candidate drug for clinical applications in the future.



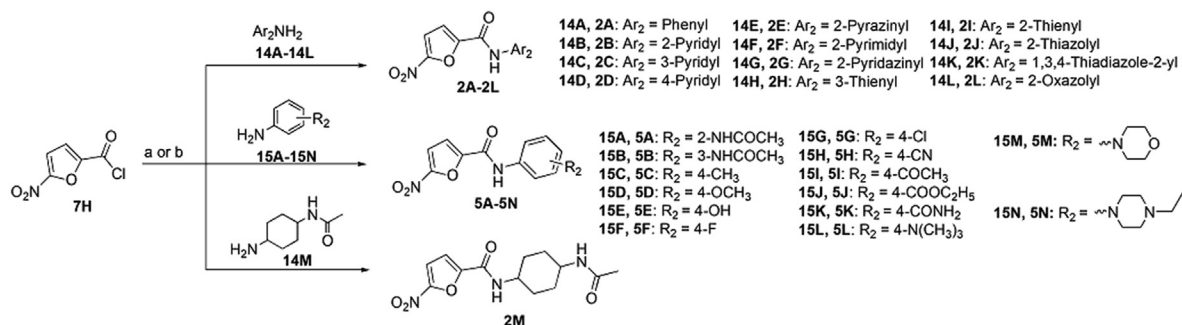
**Scheme 1** Synthesis method of compounds **1A–1H** and **4A–4D**. Reagents and conditions: (a) (COCl)<sub>2</sub>, DMF, CH<sub>2</sub>Cl<sub>2</sub>, r.t., 2 h; (b) Et<sub>3</sub>N, THF, r.t., 2–5 h.

### 2.13. UT-A1 selective inhibition activity of **1H**

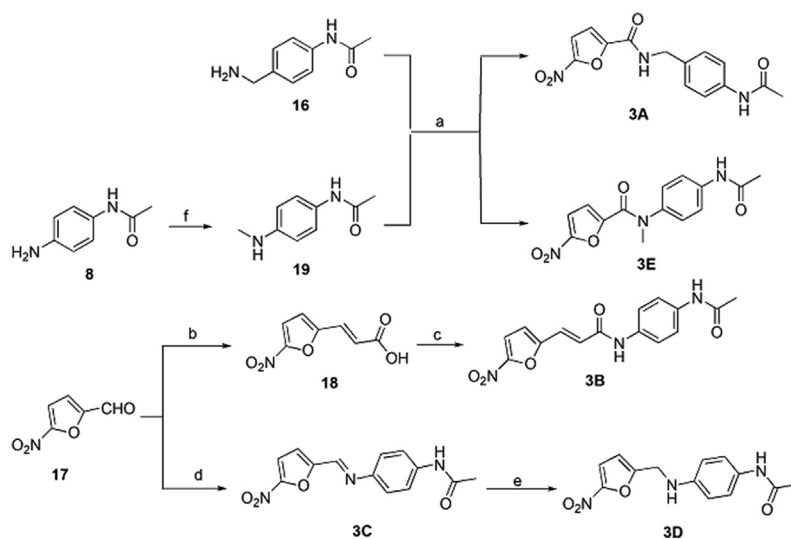
To measure the IC<sub>50</sub> against rat UT-A1, MDCK cell lines stably expressing rat UT-A1 were used. The IC<sub>50</sub> of **1H** against rat UT-A1 was 0.09 ± 0.02 μmol/L (Fig. 9A). Compared with the IC<sub>50</sub> of **1H** against rat UT-B (0.64 ± 0.20 μmol/L), we concluded that **1H** exhibited higher inhibitory activity against UT-A1 than UT-B (Fig. 9B). To further confirm this conclusion, UT-A1 knockout mice and UT-B knockout mice<sup>13</sup> were treated with 100 mg/kg **1H** by intragastric administration. The urine output obviously increased (Fig. 9C) at 2nd h after **1H** administration in UT-B knockout mice, and the urinary osmolality correspondingly decreased in UT-B knockout mice (Fig. 9D). However, the urine output and urinary osmolality did not change significantly in UT-A1 knockout mice (Fig. 9C and D). As UT-A1 was more suitable as a diuretic target than UT-B, **1H** was more likely to be developed as a novel diuretic.



**Scheme 2** Synthesis route of intermediates **6K** and **6L**. Reagents and conditions: (a) Pd/C, H<sub>2</sub>, MeOH, r.t., 2 h; (b) (CH<sub>3</sub>CO)<sub>2</sub>O, r.t., 1 h; (c) LiOH, MeOH/H<sub>2</sub>O, r.t., 15 min; (d) CH<sub>3</sub>SO<sub>2</sub>Na, DMSO, 110 °C, 20 h.

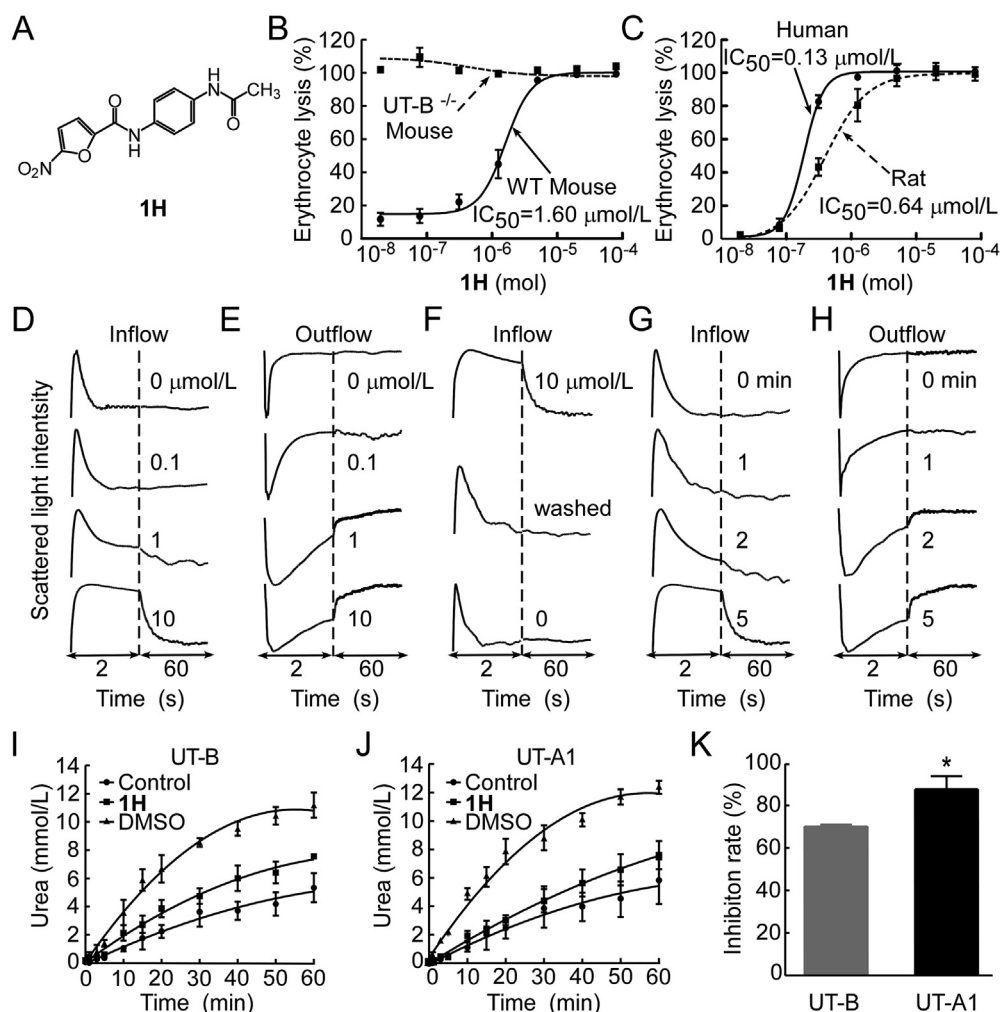


**Scheme 3** Synthesis route of **2A–2M** and **5A–5N**. Reagents and conditions: (a) Et<sub>3</sub>N, THF, r.t., 2–5 h; (b) DIEA, ClCH<sub>2</sub>CH<sub>2</sub>Cl, 60 °C, overnight.



**Scheme 4** Synthesis route of **3A–3E**. Reagents and conditions: (a) **7h**, Et<sub>3</sub>N, THF, r.t., 2 h; (b) CH<sub>2</sub>(COOH)<sub>2</sub>, pyridine, reflux, 2 h; (c) **8**, EDCl, HOBT, DIEA, CH<sub>2</sub>Cl<sub>2</sub>, overnight; (d) **8**, anhydrous MgSO<sub>4</sub>, CH<sub>2</sub>Cl<sub>2</sub>, r.t., 2 h; (e) NaBH<sub>4</sub>, MeOH, r.t., overnight; (f) (HCHO)<sub>m</sub>, MeONa, MeOH, reflux, 2 h; NaBH<sub>4</sub>, MeOH, r.t., overnight.





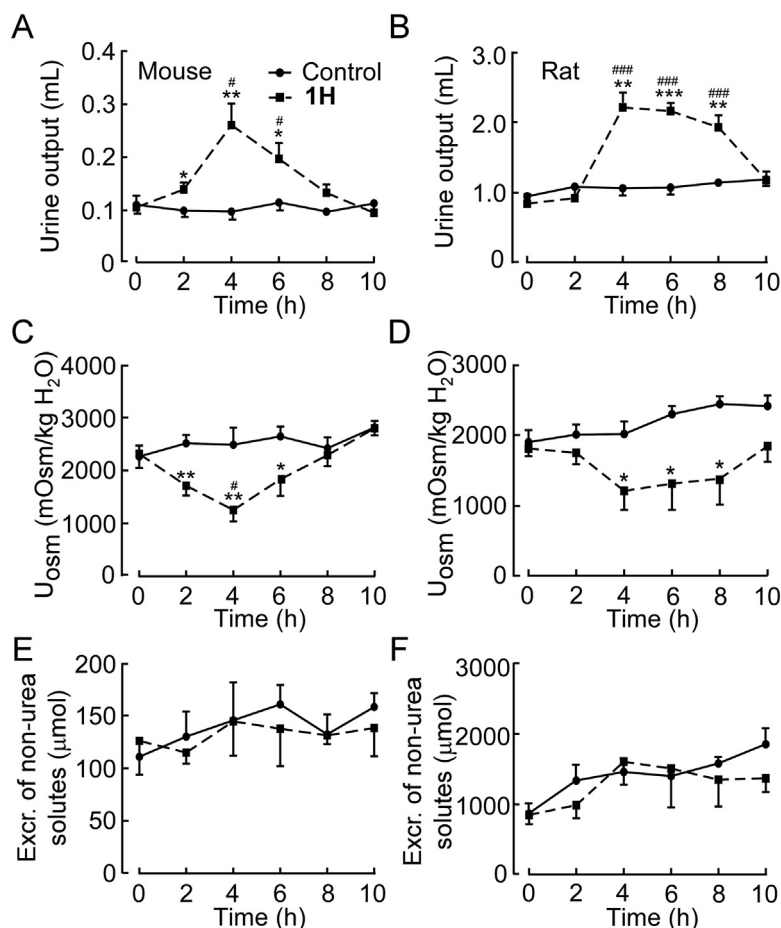
**Figure 4** Inhibition activity of **1H** on UT-B and UT-A1. (A) Structure of **1H**. (B) In the erythrocyte lysis assay, inhibition activity of **1H** on mouse UT-B. (C) Inhibition activity of **1H** on human and rat UT-B. (D) Effect of **1H** on UT-B-mediated urea influx measured by stopped-flow light scattering. (E) Effect of **1H** on UT-B-mediated urea efflux. (F) Reversibility of UT-B inhibition. **1H** was washed out after 5 min of incubation. (G) Inhibition of UT-B-mediated urea influx with different incubation time of **1H**. (H) Inhibition of UT-B-mediated urea efflux with different incubation time of **1H**. (I) Inhibition activity of **1H** on UT-B in MDCK cells. (J) Inhibition activity of **1H** on UT-A1 in MDCK cells. (K) Inhibition rate of **1H** on UT-B or UT-A1. Data are means  $\pm$  SEM;  $n = 3$ . \* $P < 0.05$  indicating that the inhibition rate of **1H** on urea transport of MDCK cells transfected with UT-A1 compared with that of MDCK cells transfected with UT-B.

#### 2.14. Pharmacokinetics of **1H**

The pharmacokinetic parameters of **1H** were measured both *in vitro* and *in vivo*. Membrane permeability is a key parameter to assess the absorption of oral drugs in the intestine<sup>49–52</sup>, and the apparent permeability coefficient ( $P_{\text{app}}$ ) in the Caco-2 cell model corresponds to the fraction absorbance (Fa) of oral drug administration in the human intestine. As shown in Fig. 10A, the  $P_{\text{app}}$  (A to B) of **1H** was  $(10.46 \pm 1.36) \times 10^{-6} \text{ cm/s}$  in the Caco-2 bidirectional transport assay, which was comparable to the high permeability compound metoprolol [ $(13.08 \pm 0.65) \times 10^{-6} \text{ cm/s}$ ]. The high  $P_{\text{app}}$  (A to B) value demonstrated that **1H** obtained a better membrane permeability that led to adequate oral absorption in the gastrointestinal tract. The efflux ratio of **1H** was  $2.00 \pm 0.14$  in Caco-2 cell monolayers, and the addition of the efflux transporter inhibitor GF120918 did not significantly alter the efflux

ratio (Fig. 10B), which indicates that **1H** may not be a sensitive substrate for efflux transporters, including P-glycoprotein (P-gp) and breast cancer resistance protein (BCRP).

The mean plasma concentration–time profiles of **1H** in rats are shown in Fig. 10C. **1H** was quickly absorbed after oral gavage at a 100 mg/kg dose, and the time to reach the maximum concentration ( $C_{\text{max}} = 0.26 \pm 0.12 \mu\text{mol/L}$ ) was  $0.31 \pm 0.13 \text{ h}$ . Then, the plasma concentrations slightly decreased, and the plasma half-life ( $t_{1/2}$ ) was  $0.93 \pm 0.09 \text{ h}$ . The results demonstrated that **1H** obtained a good gastric-intestinal absorption in rats. The oral bioavailability of **1H** was  $4.38 \pm 1.30\%$ , so it needs a higher dose (100 mg/kg) to exert an obvious oral activity, despite a potent UT inhibitory activity of **1H** *in vitro*. In the following project, it is necessary to further optimize the structure or improve the dosage form to increase the oral bioavailability of **1H** for its clinical applicability. Eight hours after oral administration, the mean



**Figure 5** Diuretic effect of subcutaneous injection of **1H** in mice and rats. (A) Urine output of mice. Mice were adapted in metabolic cages for three days. After collecting 2-h basal urine output (time 0), **1H** with a dose of 100 mg/kg was administrated by subcutaneous injection, and then urine samples were collected every 2 h. (B) Urine output of rats after **1H** administration. (C) Urinary osmolality of mice. (D) Urinary osmolality of rats. (E) Excretion of non-urea solutes of mice. (F) Excretion of non-urea solutes of rats. Data are means  $\pm$  SEM;  $n = 6$ . \* $P < 0.05$ , \*\* $P < 0.01$ , \*\*\* $P < 0.001$  compared with control mice or rats; # $P < 0.05$ , ### $P < 0.001$  compared with basal value.

plasma concentrations decreased to levels below the lower limit of quantification (1 ng/mL), which suggests that **1H** was rapidly and completely cleared from the rat plasma and may have other metabolism-related issues in the *in vivo* deposition process. The  $C_{max}$  was  $0.26 \pm 0.12 \mu\text{mol/L}$ , which was more than the  $IC_{50}$  against UT-A1 ( $0.09 \pm 0.02 \mu\text{mol/L}$ ) and less than the  $IC_{50}$  against UT-B ( $0.64 \pm 0.20 \mu\text{mol/L}$ ) and reached the effective concentration measured *in vitro*. Inhibiting UT-A1 rather than inhibiting UT-B is a great merit of the development of **1H** as a diuretic.

### 3. Conclusions

In this study, we discovered **1H** as a novel small molecule that inhibited both UT-A and UT-B with  $IC_{50}$  values at the sub-micromolar level and inhibited UT-A more than UT-B. For the first time, **1H** showed significant diuretic activity by oral administration without causing electrolyte imbalance. **1H** did not exhibit apparent toxicity either *in vitro* or *in vivo*. All these results suggest that **1H** might be developed as a novel diuretic to treat hyponatremia accompanied with volume expansion, such as hepatic cirrhosis, congestive heart failure, and nephrotic syndrome.

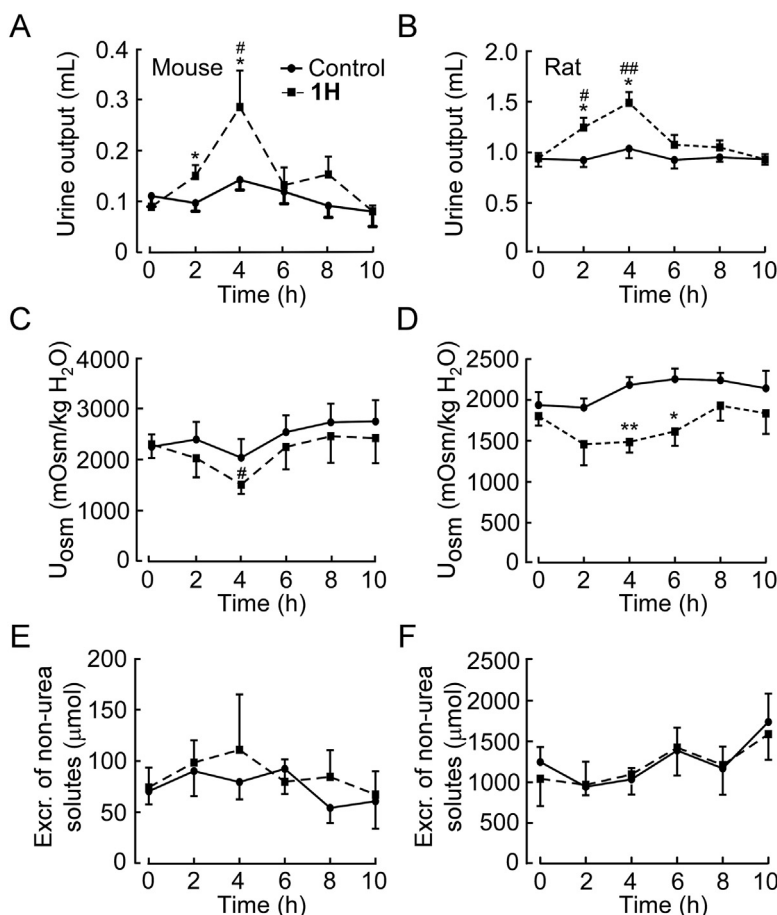
## 4. Experimental

### 4.1. Chemistry

Starting materials, solvents, and reagents were commercially available and used without further purification.  $^1\text{H}$  spectra and  $^{13}\text{C}$  spectra were recorded on a Bruker AVANCEIII 400 MHz and 100 MHz NMR spectrometer (Bruker, Karlsruhe, Germany), respectively. Chemical shifts are expressed as  $\delta$  units in ppm (in NMR description, s = singlet, d = doublet, t = triplet, q = quartet, m = multiplet, and br = broad peak). Melting points were determined on X4 microscope (Beijing, China) and uncorrected. The maximum temperature was 300  $^{\circ}\text{C}$ . HR-MS spectra were acquired by electrospray ionization (ESI) in positive ion mode using Bruker Solarix XR FTMS (Bruker).

### 4.2. Purity of primary compounds

Purity of all compounds tested in biological assays was determined to be  $>95\%$  by HPLC analysis. The following methods were used: HPLC-Agilent 1260 (Agilent Technologies Inc., Palo Alto, CA, USA), Agilent zorbax eclipse ZORBAX SB-C18



**Figure 6** Diuretic effect of intragastric administration of **1H** in mice and rats. (A) Urine output of mice. Mice were adapted in metabolic cages for three days. After collecting 2-h basal urine output (time 0), **1H** with a dose of 100 mg/kg was administrated by intragastric injection, and then urine samples were collected every 2 h. (B) Urine output of rats after **1H** administration. (C) Urinary osmolality of mice. (D) Urinary osmolality of rats. (E) Excretion of non-urea solutes of mice. (F) Excretion of non-urea solutes of rats. Data are means  $\pm$  SEM;  $n = 6$ . \* $P < 0.05$ , \*\* $P < 0.01$  compared with control mice or rats; # $P < 0.05$ , ## $P < 0.01$  compared with basal value.

(150 mm  $\times$  4.6 mm, I.D. 5  $\mu$ m), DAD (254 or 260 nm) detector, water (mobile phase A), methanol (mobile phase B), 0 min 20% B, 8 min 55% B, 20 min 80% B; or Waters e2695 (Waters, Milford, MA, USA), shim-pack VP-ODS (150 mm  $\times$  4.6 mm, I.D. 5  $\mu$ m), DAD (254 or 260 nm) detector, water (mobile phase A), methanol (mobile phase B), 0–8 min 20% B; 9 min 55% B; 20 min 80% B.

#### 4.3. General synthetic procedure A

Compounds **6A–6L** (2.0 mmol) in  $CH_2Cl_2$  (5 mL) were cooled to 0  $^{\circ}C$ . Three drops of DMF was added followed by dropping oxalyl chloride (3 mmol, 380 mg) slowly to the suspension. After 2 h of stirring at r.t., the reaction mixture was concentrated under reduced pressure to remove solvent and excessive oxalyl chloride to afford crude material of **7A–7L** without further purification.

Compound **8** (1.0 mmol, 150 mg) and  $Et_3N$  (1.5 mmol, 152 mg) in THF (5 mL) were cooled to 0  $^{\circ}C$  and then **7A–7L** prepared above in THF (2 mL) were dropped slowly to the solution. The reaction mixture was stirred for 2–5 h at r.t. After the reaction completed, water was added and the mixture was stirred for further 10 min. The precipitate was filtered, washed with water

and recrystallized with ethanol or methanol to afford the pure product.

##### 4.3.1. *N*-(4-Acetamidophenyl)benzamide (**1A**)

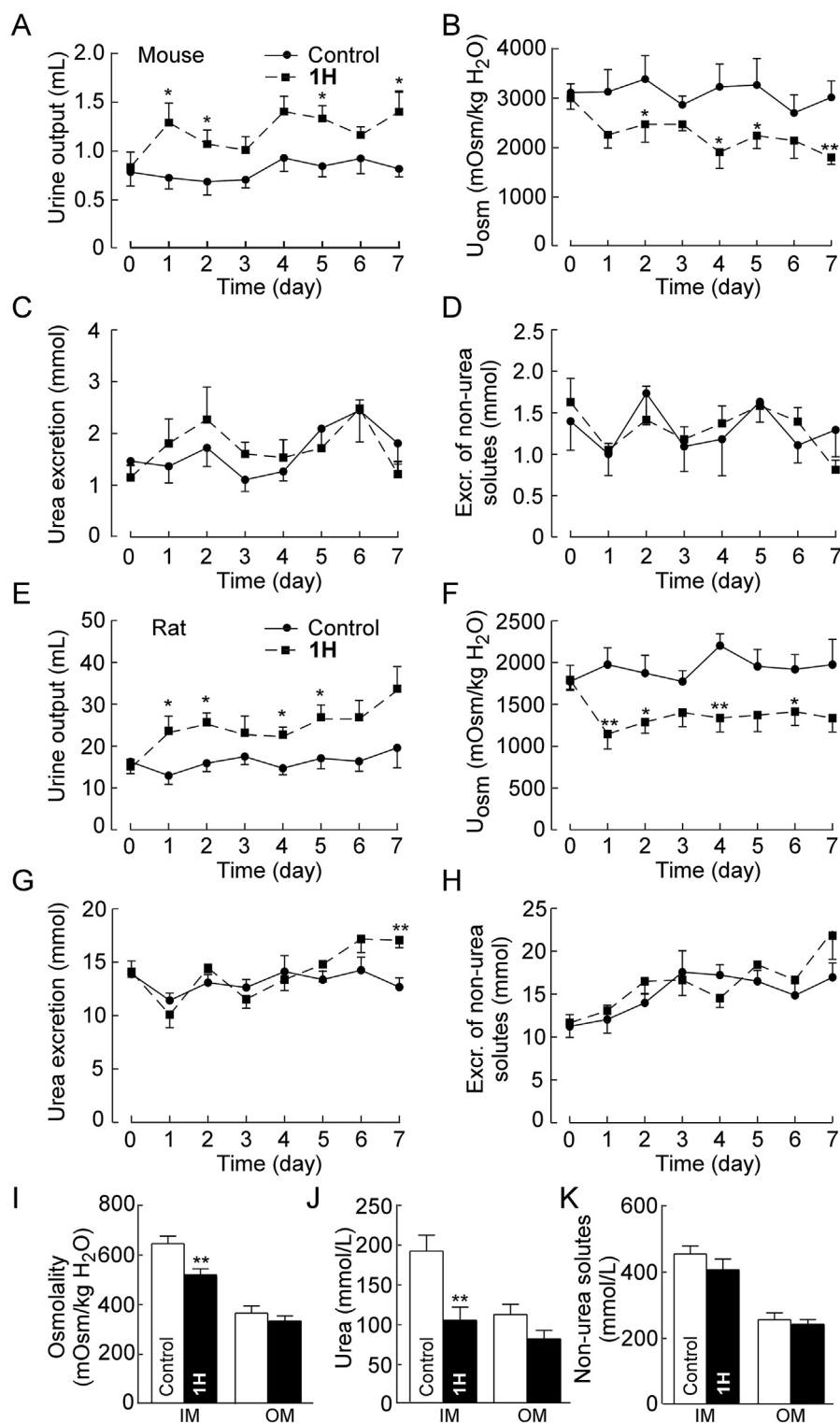
Prepared from **6A** following general synthetic procedure A. White solid; Yield 75%; m.p. 211–213  $^{\circ}C$ .

##### 4.3.2. *N*-(4-Acetamidophenyl)thiophene-2-carboxamide (**1B**)

Prepared from **6B** following general synthetic procedure A. White solid; Yield 65%; m.p. 247–248  $^{\circ}C$ .  $^1H$  NMR (400 MHz,  $DMSO-d_6$ )  $\delta$  10.17 (s, 1H), 9.91 (s, 1H), 7.99 (d,  $J = 3.5$  Hz, 1H), 7.84 (d,  $J = 4.9$  Hz, 1H), 7.62 (d,  $J = 8.8$  Hz, 2H), 7.54 (d,  $J = 8.8$  Hz, 2H), 7.22 (t,  $J = 4.3$  Hz, 1H), 2.03 (s, 3H).  $^{13}C$  NMR (101 MHz,  $DMSO-d_6$ )  $\delta$  168.57, 160.16, 140.71, 135.88, 134.34, 132.20, 129.40, 128.59, 121.43, 119.76, 24.47. HR-MS (ESI):  $m/z$  Calcd.  $C_{13}H_{12}O_2N_2S$   $[M+H]^+$ : 261.0692; Found: 261.0695.

##### 4.3.3. *N*-(4-Acetamidophenyl)furan-2-carboxamide (**1C**)

Prepared from **6C** following general synthetic procedure A. White solid; Yield 68%; m.p. 212–214  $^{\circ}C$ .  $^1H$  NMR (400 MHz,  $DMSO-d_6$ )  $\delta$  10.11 (s, 1H), 9.91 (s, 1H), 7.92 (d,  $J = 1.7$  Hz, 1H), 7.64 (d,  $J = 8.9$  Hz, 2H), 7.53 (d,  $J = 8.9$  Hz, 2H), 7.30 (d,  $J = 3.4$  Hz, 1H), 6.69 (dd,  $J = 3.4, 1.7$  Hz, 1H), 2.03 (s, 3H).  $^{13}C$  NMR



**Figure 7** Long-term diuretic effect of **1H** in mice and rats. Mice and rats were adapted in the metabolic cage for three days, and then urine was collected for 1 day as the basal level. **1H** with a dose of 100 mg/kg was given to the experimental group by gavage 3 times a day (the first dose was doubled) for consecutive 7 days. After the last dose, the renal inner medulla and outer medulla were acquired for experiments. (A) Urine output of mice. (B) Urine osmolality of mice. (C) Urea excretion of mice. (D) Excretion of non-urea solutes of mice. (E) Urine output of rats. (F) Urine osmolality of rats. (G) Urea excretion of rats. (H) Excretion of non-urea solutes of rats. (I) Osmolality of the inner medulla (IM) and outer medulla (OM) interstitial fluid of rats. (J) Urea concentration of rats. (K) Concentration of non-urea solutes of rats. Data are means  $\pm$  SEM;  $n = 8$ . \* $P < 0.05$ , \*\* $P < 0.01$  compared with control.

**Table 6** Body weight, kidney index and blood chemistry in control or **1H**-treated rats.

Measured parameters	Control	<b>1H</b> <sup>a</sup>
Body weight (g)	276.2 ± 18.7	281.9 ± 5.0
Kidney index (%)	0.82 ± 0.09	0.85 ± 0.03
Serum urea (mmol/L)	7.03 ± 0.34	7.05 ± 0.43
Serum creatinine (μmol/L)	33.9 ± 2.9	34.6 ± 8.3
Serum Na (mmol/L)	146.7 ± 2.0	147.3 ± 2.0
Serum K (mmol/L)	4.6 ± 0.1	4.8 ± 0.2
Serum Cl (mmol/L)	102.0 ± 1.5	101.7 ± 1.3
Serum triglyceride (mmol/L)	0.54 ± 0.05	0.68 ± 0.07
Serum HDL-C (mmol/L)	0.70 ± 0.02	0.71 ± 0.03
Serum LDL-C (mmol/L)	0.35 ± 0.03	0.34 ± 0.03
Serum glucose (mmol/L)	9.0 ± 0.3	9.4 ± 0.3
Serum cholesterol (mmol/L)	1.63 ± 0.07	1.59 ± 0.06

*P* < 0.05 compared with control rats.

<sup>a</sup>Data are means ± SEM, *n* = 8.

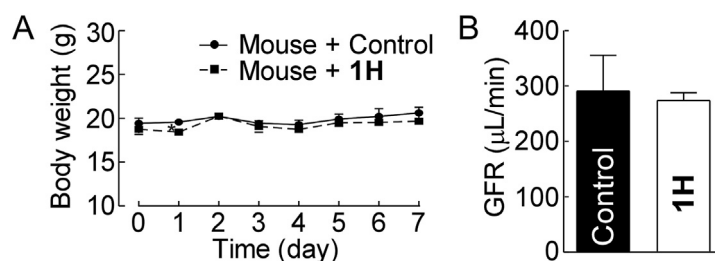
(101 MHz, DMSO-*d*<sub>6</sub>) δ 168.46, 156.44, 148.06, 146.02, 135.77, 134.07, 121.28, 119.65, 114.89, 112.55, 24.37. HR-MS (ESI): *m/z* Calcd. C<sub>13</sub>H<sub>12</sub>O<sub>2</sub>N<sub>3</sub> [M+H]<sup>+</sup>: 245.0921; Found: 245.0913.

#### 4.3.4. *N*-(4-Acetamidophenyl)-1*H*-pyrrole-2-carboxamide (**1D**)

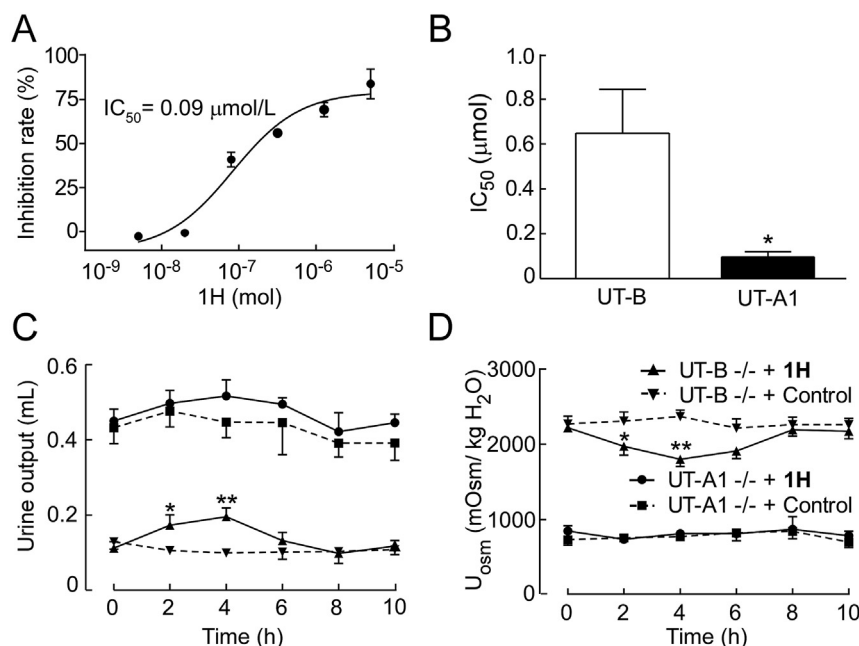
Prepared from **6D** following general synthetic procedure A. White solid; Yield 66%; m.p. 260–262 °C. <sup>1</sup>H NMR (400 MHz, DMSO-*d*<sub>6</sub>) δ 11.61 (s, 1H), 9.87 (s, 1H), 9.68 (s, 1H), 7.62 (d, *J* = 8.8 Hz, 2H), 7.51 (d, *J* = 8.8 Hz, 2H), 7.03 (s, 1H), 6.94 (s, 1H), 6.15 (d, *J* = 2.9 Hz, 1H), 2.03 (s, 3H). <sup>13</sup>C NMR (101 MHz, DMSO-*d*<sub>6</sub>) δ 168.37, 159.39, 135.13, 134.95, 126.56, 122.77, 120.80, 119.70, 111.50, 109.27, 24.35. HR-MS (ESI) *m/z*: Calcd. C<sub>13</sub>H<sub>14</sub>N<sub>3</sub>O<sub>2</sub> [M+H]<sup>+</sup>: 244.1081; Found: 244.1085.

#### 4.3.5. *N*-(4-Acetamidophenyl)oxazole-5-carboxamide (**1E**)

Prepared from **6E** following general synthetic procedure A. White solid; Yield 72%; m.p. 255–257 °C. <sup>1</sup>H NMR (400 MHz, DMSO-

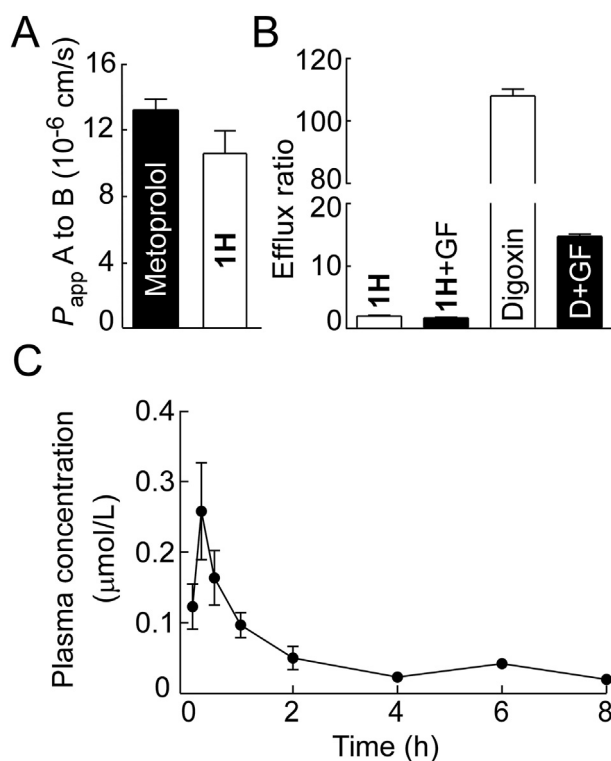


**Figure 8** Toxicity assessments of **1H**. Mice were adapted in the metabolic cage for three days. **1H** with a dose of 100 mg/kg was given to the experimental group by gavage 3 times a day (the first dose was doubled) for consecutive 7 days. The body weight and the GFR were measured. (A) Body weight, *n* = 8. (B) glomerular filtration rate (GFR), *n* = 4. Data are means ± SEM. \**P* < 0.05 compared with control mice.



**Figure 9** Selective inhibition activity of **1H** on UT-A1. (A) Inhibition activity of **1H** on rat UT-A1 determined with MDCK cells expressing rat UT-A1. (B) Calculated IC<sub>50</sub> of **1H** on rat UT-B and UT-A1. (C) Urine output of UT-A1 and UT-B knockout mice. Mice were adapted in the metabolic cage for three days. After collecting 2-h basal urine output (time 0), **1H** with a dose of 100 mg/kg was administrated by intragastric injection, and then urine samples were collected every 2 h. (D) Urinary osmolality of UT-A1 and UT-B knockout mice, *n* = 6. Data are means ± SEM. \**P* < 0.05, \*\**P* < 0.01 compared with control mice.





**Figure 10** Pharmacokinetics of **1H**. (A) The apparent permeability of **1H** in the Caco-2 cell. (B) The efflux ratio of **1H** in Caco-2 cell monolayers. (C) Plasma concentration–time profiles of **1H** in rats. Data are means  $\pm$  SEM,  $n = 3$ .

$d_6$ )  $\delta$  10.37 (s, 1H), 9.94 (s, 1H), 8.64 (s, 1H), 7.96 (s, 1H), 7.63 (d,  $J = 9.0$  Hz, 2H), 7.56 (d,  $J = 9.0$  Hz, 2H), 2.04 (s, 3H).  $^{13}\text{C}$  NMR (101 MHz, DMSO- $d_6$ )  $\delta$  168.55, 155.16, 154.21, 145.74, 136.17, 133.59, 130.29, 121.45, 119.71, 24.39. HR-MS  $m/z$ : Calcd.  $\text{C}_{12}\text{H}_{14}\text{N}_3\text{O}_3$   $[\text{M}+\text{H}]^+$ : 246.0873; Found: 246.0868.

#### 4.3.6. *N*-(4-Acetamidophenyl)picolinamide (**1F**)

Prepared from **6F** following general synthetic procedure A. White solid; Yield 70%; m.p. 165–166 °C.  $^1\text{H}$  NMR (400 MHz, DMSO- $d_6$ )  $\delta$  10.56 (s, 1H), 9.93 (s, 1H), 8.73 (d,  $J = 4.3$  Hz, 1H), 8.15 (d,  $J = 7.8$  Hz, 1H), 8.07 (td,  $J = 7.8, 1.6$  Hz, 1H), 7.82 (d,  $J = 8.9$  Hz, 2H), 7.67 (td,  $J = 6.0, 1.2$  Hz, 1H), 7.56 (d,  $J = 8.9$  Hz, 2H), 2.04 (s, 3H).  $^{13}\text{C}$  NMR (101 MHz, DMSO- $d_6$ )  $\delta$  168.48, 162.59, 150.43, 148.85, 138.57, 135.90, 133.97, 127.28, 122.73, 121.08, 119.67, 24.38. HR-MS  $m/z$ : Calcd.  $\text{C}_{12}\text{H}_{14}\text{N}_3\text{O}_3$   $[\text{M}+\text{H}]^+$ : 256.1081; Found: 256.1074.

#### 4.3.7. *N*-(4-Acetamidophenyl)benzofuran-2-carboxamide (**1G**)

Prepared from **6G** following general synthetic procedure A. White solid; Yield 62%; m.p. 257–258 °C.  $^1\text{H}$  NMR (400 MHz, DMSO- $d_6$ )  $\delta$  10.48 (s, 1H), 9.95 (s, 1H), 7.83 (d,  $J = 7.8$  Hz, 1H), 7.79–7.64 (m, 4H), 7.57 (d,  $J = 8.8$  Hz, 2H), 7.51 (t,  $J = 7.8$  Hz, 1H), 7.37 (t,  $J = 7.8$  Hz, 1H), 2.04 (s, 3H).  $^{13}\text{C}$  NMR (101 MHz, DMSO- $d_6$ )  $\delta$  168.54, 156.85, 154.87, 149.35, 136.05, 133.89, 127.62, 127.54, 124.29, 123.34, 121.42, 119.67, 112.38, 110.87, 24.38. HR-MS  $m/z$ : Calcd.  $\text{C}_{17}\text{H}_{15}\text{N}_2\text{O}_3$   $[\text{M}+\text{H}]^+$ : 295.1077; Found: 295.1080.

**4.3.8. *N*-(4-Acetamidophenyl)-5-nitrofuran-2-carboxamide (**1H**)**  
Prepared from **6H** following general synthetic procedure A. Orange solid; Yield 80%; m.p. 233–234 °C.  $^1\text{H}$  NMR (400 MHz, DMSO- $d_6$ )  $\delta$  10.59 (s, 1H), 9.97 (s, 1H), 7.81 (d,  $J = 4.0$  Hz, 1H), 7.62–7.66 (m, 3H), 7.57 (d,  $J = 8.8$  Hz, 2H), 2.04 (s, 3H).  $^{13}\text{C}$  NMR (101 MHz, DMSO- $d_6$ )  $\delta$  168.61, 154.79, 152.20, 148.56, 136.49, 133.32, 121.66, 119.71, 116.77, 113.97, 24.40. HR-MS  $m/z$ : Calcd.  $\text{C}_{13}\text{H}_{13}\text{N}_3\text{O}_5$   $[\text{M}+\text{H}]^+$ : 290.0772; Found: 290.0766.

#### 4.3.9. *N*-(4-Acetamidophenyl)-5-methylfuran-2-carboxamide (**4A**)

Prepared from **6I** following general synthetic procedure A. Light yellow solid; Yield 88%; m.p. 183–184 °C.  $^1\text{H}$  NMR (400 MHz,  $\text{CDCl}_3$ )  $\delta$  7.99 (s, 1H), 7.59 (d,  $J = 8.0$  Hz, 2H), 7.49 (d,  $J = 8.0$  Hz, 2H), 7.34 (s, 1H), 7.13 (s, 1H), 6.16 (s, 1H), 2.41 (s, 3H), 2.18 (s, 3H).  $^{13}\text{C}$  NMR (101 MHz,  $\text{CDCl}_3$ )  $\delta$  168.25, 156.18, 154.99, 146.09, 134.33, 133.77, 120.60, 116.58, 109.09, 24.53, 13.94. HR-MS  $m/z$ : Calcd.  $\text{C}_{14}\text{H}_{15}\text{N}_2\text{O}_3$   $[\text{M}+\text{H}]^+$ : 259.1077; Found: 259.1074.

#### 4.3.10. *N*-(4-Acetamidophenyl)-5-bromofuran-2-carboxamide (**4B**)

Prepared from **6J** following general synthetic procedure A. Light yellow solid; Yield 85%; m.p. 217–219 °C.  $^1\text{H}$  NMR (400 MHz, DMSO- $d_6$ )  $\delta$  10.15 (s, 1H), 9.92 (s, 1H), 7.62 (d,  $J = 9.0$  Hz, 2H), 7.53 (d,  $J = 9.0$  Hz, 2H), 7.34 (d,  $J = 3.6$  Hz, 1H), 6.83 (d,  $J = 3.6$  Hz, 1H), 2.03 (s, 3H).  $^{13}\text{C}$  NMR (101 MHz, DMSO- $d_6$ )  $\delta$  168.50, 155.35, 149.84, 135.94, 133.81, 125.61, 121.39, 119.67, 117.32, 114.69, 24.38. HR-MS  $m/z$ : Calcd.  $\text{C}_{13}\text{H}_{12}\text{BrN}_2\text{O}_3$   $[\text{M}+\text{H}]^+$ : 323.0026; Found: 323.0022.

#### 4.3.11. *N*-(4-Acetamidophenyl)-5-acetamidofuran-2-carboxamide (**4C**)

Prepared from **6K** following general synthetic procedure A. Light yellow solid; Yield 58%; m.p. 251–253 °C.  $^1\text{H}$  NMR (400 MHz, DMSO- $d_6$ )  $\delta$  11.40 (s, 1H), 9.92 (s, 1H), 9.88 (s, 1H), 7.61 (d,  $J = 9.0$  Hz, 2H), 7.55 (d,  $J = 9.0$  Hz, 2H), 7.43 (d,  $J = 3.6$  Hz, 1H), 6.37 (d,  $J = 3.6$  Hz, 1H), 2.08 (s, 3H), 2.05 (s, 3H).  $^{13}\text{C}$  NMR (101 MHz, DMSO- $d_6$ )  $\delta$  168.43, 167.38, 156.40, 149.89, 139.31, 135.50, 134.38, 120.91, 119.73, 116.91, 24.36, 23.41.

#### 4.3.12. *N*-(4-Acetamidophenyl)-5-(methylsulfonyl)furan-2-carboxamide (**4D**)

Prepared from **6L** following general synthetic procedure A. Pale white solid; Yield 47%; m.p. 251–253 °C.  $^1\text{H}$  NMR (400 MHz, DMSO- $d_6$ )  $\delta$  10.40 (s, 1H), 9.96 (s, 1H), 7.62 (d,  $J = 8.8$  Hz, 2H), 7.57 (d,  $J = 8.8$  Hz, 2H), 7.48 (d,  $J = 3.6$  Hz, 1H), 7.44 (d,  $J = 3.6$  Hz, 1H), 3.43 (s, 3H), 2.04 (s, 3H).  $^{13}\text{C}$  NMR (101 MHz, DMSO- $d_6$ )  $\delta$  168.58, 155.31, 151.01, 150.91, 136.39, 133.32, 121.76, 119.70, 118.23, 115.31, 43.28, 24.40. HR-MS  $m/z$ : Calcd.  $\text{C}_{14}\text{H}_{15}\text{N}_2\text{O}_5\text{S}$   $[\text{M}+\text{H}]^+$ : 323.0696; Found: 323.0690.

### 4.4. General synthetic procedure B

Amines (**14A**, **14H**–**14M**, **15A**–**15N**, **16** or **19**, 1.0 mmol) and  $\text{Et}_3\text{N}$  (1.5 mmol, 152 mg) in THF (5 mL) were cooled to 0 °C, and then **7H** (1.0 mmol, 175 mg) in THF (2 mL) was dropped slowly to the solution. The reaction mixture was stirred for 2–5 h at r.t. After the reaction completed, water was added and the mixture was stirred for further 10 min. The precipitate was filtered, washed

with water and recrystallized with ethanol or methanol to afford the pure products.

#### 4.4.1. 5-Nitro-*N*-phenylfuran-2-carboxamide (**2A**)

Prepared from **14A** following general synthetic procedure B. Yellow solid; Yield 73%; m.p. 178–180 °C. <sup>1</sup>H NMR (400 MHz, DMSO-*d*<sub>6</sub>) δ 10.63 (s, 1H), 7.82 (d, *J* = 3.9 Hz, 1H), 7.74 (d, *J* = 7.7 Hz, 2H), 7.64 (d, *J* = 3.9 Hz, 1H), 7.39 (t, *J* = 7.9 Hz, 2H), 7.17 (t, *J* = 7.4 Hz, 1H). <sup>13</sup>C NMR (101 MHz, DMSO-*d*<sub>6</sub>) δ 165.05, 152.22, 148.39, 138.26, 129.29, 125.04, 121.17, 116.98, 113.93. HR-MS *m/z*: Calcd. C<sub>11</sub>H<sub>8</sub>N<sub>2</sub>O<sub>4</sub> [M+H]<sup>+</sup>: 233.0557, Found: 233.0552.

#### 4.4.2. 5-Nitro-*N*-(thiophen-3-yl)furan-2-carboxamide (**2H**)

Prepared from **14H** following general synthetic procedure B. Yellow solid; Yield 75%; m.p. 214–215 °C. <sup>1</sup>H NMR (400 MHz, DMSO-*d*<sub>6</sub>) δ 11.11 (s, 1H), 7.81 (s, 1H), 7.74 (s, 1H), 7.58 (d, *J* = 2.6 Hz, 1H), 7.53 (t, *J* = 2.6 Hz, 1H), 7.34 (d, *J* = 5.0 Hz, 1H). <sup>13</sup>C NMR (101 MHz, DMSO-*d*<sub>6</sub>) δ 154.21, 152.21, 148.31, 136.07, 125.57, 122.41, 116.88, 114.03, 111.54. HR-MS *m/z*: Calcd. C<sub>9</sub>H<sub>7</sub>N<sub>2</sub>O<sub>4</sub>S [M+H]<sup>+</sup>: 239.0121; Found: 239.0121.

#### 4.4.3. 5-Nitro-*N*-(thiophen-2-yl)furan-2-carboxamide (**2I**)

Prepared from **14I** following general synthetic procedure B. Yellow solid; Yield 67%; m.p. 212–214 °C. <sup>1</sup>H NMR (400 MHz, DMSO-*d*<sub>6</sub>) δ 12.01 (s, 1H), 7.82 (d, *J* = 4.0 Hz, 1H), 7.60 (d, *J* = 4.0 Hz, 1H), 7.10 (d, *J* = 5.4 Hz, 1H), 7.02 (d, *J* = 3.1 Hz, 1H), 6.94 (dd, *J* = 5.4 Hz, 4.0 Hz, 1H). <sup>13</sup>C NMR (101 MHz, DMSO-*d*<sub>6</sub>) δ 153.14, 152.33, 147.58, 139.05, 124.88, 119.04, 117.31, 114.08, 114.04. HR-MS *m/z*: Calcd. C<sub>9</sub>H<sub>7</sub>N<sub>2</sub>O<sub>4</sub>S [M+H]<sup>+</sup>: 239.0121; Found: 239.0116.

#### 4.4.4. 5-Nitro-*N*-(thiazol-2-yl)furan-2-carboxamide (**2J**)

Prepared from **14J** following general synthetic procedure B. Brown solid; Yield 75%; m.p. 265–268 °C. <sup>1</sup>H NMR (400 MHz, DMSO-*d*<sub>6</sub>) δ 13.32 (s, 1H), 7.81 (d, *J* = 3.6 Hz, 1H), 7.73 (s, 1H), 7.60 (d, *J* = 3.6 Hz, 1H), 7.31 (d, *J* = 3.6 Hz, 1H). <sup>13</sup>C NMR (101 MHz, DMSO-*d*<sub>6</sub>) δ 161.32, 157.25, 152.58, 148.23, 134.85, 117.77, 114.33, 113.85. HR-MS *m/z*: Calcd. C<sub>8</sub>H<sub>6</sub>N<sub>3</sub>O<sub>4</sub>S [M+H]<sup>+</sup>: 240.0074; Found: 240.0072.

#### 4.4.5. 5-Nitro-*N*-(1,3,4-thiadiazol-2-yl)furan-2-carboxamide (**2K**)

Prepared from **14K** following general synthetic procedure B. Brown solid; Yield 68%; m.p. 235–237 °C. <sup>1</sup>H NMR (400 MHz, DMSO-*d*<sub>6</sub>) δ 13.83 (br, 1H), 9.24 (s, 1H), 7.83 (s, 2H). HR-MS *m/z*: Calcd. C<sub>7</sub>H<sub>5</sub>N<sub>4</sub>O<sub>4</sub>S [M+H]<sup>+</sup>: 241.0026; Found: 241.0025.

#### 4.4.6. 5-Nitro-*N*-(oxazol-2-yl)furan-2-carboxamide (**2L**)

Prepared from **14L** following general synthetic procedure B. Brown solid; Yield 73%; m.p. 251 °C (decomposed). <sup>1</sup>H NMR (400 MHz, DMSO-*d*<sub>6</sub>) δ 12.38 (s, 1H), 7.90 (s, 1H), 7.76 (s, 1H), 7.53 (s, 1H), 7.30 (s, 1H). <sup>13</sup>C NMR (101 MHz, DMSO-*d*<sub>6</sub>) δ 152.38, 117.74, 113.88. HR-MS *m/z*: Calcd. C<sub>8</sub>H<sub>6</sub>N<sub>3</sub>O<sub>5</sub> [M+H]<sup>+</sup>: 224.0302; Found: 224.0299.

#### 4.4.7. *N*-(4-Acetamidocyclohexyl)-5-nitrofuran-2-carboxamide (**2M**)

Prepared from **14M** following general synthetic procedure B. White solid; Yield 62%; m.p. 283–286 °C. <sup>1</sup>H NMR (400 MHz, DMSO-*d*<sub>6</sub>) δ 8.69 (d, *J* = 7.9 Hz, 1H), 7.77–7.74 (m, 2H), 7.41 (d, *J* = 3.8 Hz, 1H), 3.73 (d, *J* = 7.8 Hz, 1H), 3.48 (d,

*J* = 7.8 Hz, 1H), 1.88–1.73 (m, 7H), 1.43 (dd, *J* = 23.4, 11.8 Hz, 2H), 1.24 (dd, *J* = 23.4, 11.8 Hz, 2H). <sup>13</sup>C NMR (101 MHz, DMSO-*d*<sub>6</sub>) δ 168.71, 155.77, 151.86, 148.86, 115.88, 113.90, 48.19, 47.42, 31.61, 31.16, 23.19. HR-MS *m/z*: Calcd. C<sub>13</sub>H<sub>18</sub>N<sub>3</sub>O<sub>5</sub> [M+H]<sup>+</sup>: 296.1241; Found: 296.1241.

#### 4.4.8. *N*-(4-Acetamidobenzyl)-5-nitrofuran-2-carboxamide (**3A**)

Prepared from compound **16** following general synthetic procedure B. Yellow solid; Yield 80%; m.p. 238–240 °C. <sup>1</sup>H NMR (400 MHz, DMSO-*d*<sub>6</sub>) δ 9.94 (s, 1H), 9.41 (t, *J* = 6.0 Hz, 1H), 7.77 (d, *J* = 3.9 Hz, 1H), 7.53 (d, *J* = 8.5 Hz, 2H), 7.44 (d, *J* = 3.9 Hz, 1H), 7.24 (d, *J* = 8.5 Hz, 2H), 4.40 (d, *J* = 6.0 Hz, 2H), 2.02 (s, 3H). <sup>13</sup>C NMR (101 MHz, DMSO-*d*<sub>6</sub>) δ 168.65, 156.50, 151.94, 148.67, 138.74, 133.62, 128.35, 119.37, 116.10, 113.94, 42.38, 24.42. HR-MS *m/z*: Calcd. C<sub>14</sub>H<sub>14</sub>N<sub>3</sub>O<sub>5</sub> [M+H]<sup>+</sup>: 304.0928; Found: 304.0927.

#### 4.4.9. *N*-(4-Acetamidobenzyl)-3-(5-nitrofuran-2-yl)acrylamide (**3B**)

A mixture of 5-nitrofuran-2-carbaldehyde (**17**, 282 mg, 2 mmol), malonic acid (208 mg, 2 mmol) and pyridine (1 mL) was refluxed for 2 h. After cooled to r.t., the reaction mixture was diluted with water (20 mL). Ammonia water was added until all the solid dissolved. The mixture was filtered and the filtrate was adjusted to pH 3–4 with 4 mol/L hydrochloric acid. Yellow solid was precipitated, filtered and dried to yield compound **18** (275 mg, 1.5 mmol, 75%). A mixture of compound **18** (275 mg, 1.5 mmol, 1.0 equiv.), compound **8** (225 mg, 1.5 mmol/L, 1.0 equiv.), EDCI (316 mg, 1.65 mmol, 1.1 equiv.), 1-hydroxybenzotriazole (HOBt, 223 mg, 1.65 mmol, 1.1 equiv.) and *N,N*-diisopropylethylamine (DIEA, 291 mg, 2.25 mmol, 1.5 equiv.) in CH<sub>2</sub>Cl<sub>2</sub> (5 mL) was stirred overnight at r.t. After the solvent removed, the residue was slurried with 2 mol/L hydrochloric acid (5 mL) for 1 h. The mixture was filtered to afford the title compound. Orange solid; Yield 70%; m.p. >300 °C (decomposed). <sup>1</sup>H NMR (400 MHz, DMSO-*d*<sub>6</sub>) δ 10.45 (s, 1H), 9.95 (s, 1H), 7.78 (d, *J* = 4.0 Hz, 1H), 7.62 (d, *J* = 9.2 Hz, 2H), 7.54 (d, *J* = 9.2 Hz, 2H), 7.46 (d, *J* = 16.0 Hz, 1H), 7.29 (d, *J* = 4.0 Hz, 1H), 6.98 (d, *J* = 16.0 Hz, 1H), 2.03 (s, 3H). <sup>13</sup>C NMR (101 MHz, DMSO-*d*<sub>6</sub>) δ 168.48, 162.23, 153.65, 152.12, 135.78, 134.61, 126.38, 125.71, 119.99, 119.85, 117.08, 115.26, 24.38. HR-MS *m/z*: Calcd. C<sub>15</sub>H<sub>14</sub>N<sub>3</sub>O<sub>5</sub> [M+H]<sup>+</sup>: 316.0928; Found: 316.0926.

#### 4.4.10. *N*-(4-(((5-Nitrofuran-2-yl)methylene)amino)phenyl)acetamide (**3C**)

A mixture of compound **17** (141 mg, 1 mmol), compound **8** (150 mg, 1 mmol) and anhydrous MgSO<sub>4</sub> (60 mg, 0.5 mmol) was stirred at room temperature for 2 h. Red solid precipitated, filtered and dried to afford the title compound. Yield 70%; m.p. 230–233 °C. <sup>1</sup>H NMR (400 MHz, DMSO-*d*<sub>6</sub>) δ 10.11 (s, 1H), 8.65 (s, 1H), 7.83 (d, *J* = 3.8 Hz, 1H), 7.67 (d, *J* = 8.6 Hz, 2H), 7.40 (m, 3H), 3.05 (s, 3H). <sup>13</sup>C NMR (101 MHz, DMSO-*d*<sub>6</sub>) δ 168.88, 153.65, 152.70, 144.78, 139.67, 122.77, 119.97, 117.80, 114.79, 24.51. HR-MS *m/z*: Calcd. C<sub>13</sub>H<sub>12</sub>N<sub>3</sub>O<sub>4</sub> [M+H]<sup>+</sup>: 274.0822; Found: 274.0817.

#### 4.4.11. *N*-(4-(((5-Nitrofuran-2-yl)methyl)amino)phenyl)acetamide (**3D**)

NaBH<sub>4</sub> was added in batches to a solution of compound **3C** (180 mg, 0.66 mmol) and methanol (5 mL). The mixture was stirred at r.t. overnight. Water (5 mL) was added. The resulted mixture was stirred for further 30 min and filtered. The filtrate was

extracted with ethyl acetate (5 mL  $\times$  3). The organic layer was dried over anhydrous  $\text{Na}_2\text{SO}_4$ , filtered and concentrated. Ethanol (2 mL) following by 5 drops of 36% hydrochloric acid to the residue were added. After cooled at 4 °C for 2 h, yellow crystals were precipitated as the hydrochloride of compound **3D** which was afforded by filtration. Yield 60%; m.p. 159–161 °C.  $^1\text{H}$  NMR (400 MHz, MeOD)  $\delta$  7.69 (d,  $J$  = 8.6 Hz, 2H), 7.44 (d,  $J$  = 3.6 Hz, 1H), 7.29 (d,  $J$  = 8.6 Hz, 2H), 6.79 (d,  $J$  = 3.6 Hz, 1H), 4.77 (s, 2H), 2.13 (s, 3H).  $^{13}\text{C}$  NMR (101 MHz, MeOD)  $\delta$  170.45, 152.68, 149.02, 138.87, 131.34, 123.10, 121.72, 120.88, 120.74, 115.29, 111.71, 45.92, 22.40. HR-MS  $m/z$ : Calcd.  $\text{C}_{13}\text{H}_{14}\text{N}_3\text{O}_4$   $[\text{M}+\text{H}]^+$ : 276.0979; Found: 276.0979.

#### 4.4.12. *N*-(4-Acetamidophenyl)-*N*-methyl-5-nitrofur-2-carboxamide (**3E**)

A mixture of compound **8** (300 mg, 2 mmol), paraformaldehyde (300 mg, 10 mmol) and MeONa (540 mg, 10 mmol) in methanol (30 mL) was refluxed. The reaction was monitored by TLC ( $\text{CH}_2\text{Cl}_2/\text{MeOH}$  = 10:1, v/v) until compound **8** was reacted completely. The reaction mixture was cooled to r.t. and  $\text{NaBH}_4$  (152 mg, 4 mmol) was added in batches. The resulted mixture was stirred overnight at ambient temperature. Solvent was removed. The residue was diluted with 2 mol/L hydrochloric acid (5 mL) and ethyl acetate (5 mL). The two layers were separated. The aqueous layer was adjusted with saturated  $\text{Na}_2\text{CO}_3$  solution to pH 9 and extracted with ethyl acetate (5 mL  $\times$  3). The combined organic layers were washed with brine, dried over anhydrous  $\text{Na}_2\text{SO}_4$ , filtered and concentrated. The residue was purified by column chromatography (silica gel,  $\text{CH}_2\text{Cl}_2/\text{MeOH}$  = 80:1, v/v) to afford compound **19** as white solid (250 mg, 76% Yield). The title compound **3E** was prepared from compound **19** following general synthetic procedure B. Yield 72%; m.p. 81–83 °C.  $^1\text{H}$  NMR (400 MHz, DMSO- $d_6$ )  $\delta$  10.15 (s, 1H), 7.65 (d,  $J$  = 8.7 Hz, 2H), 7.52 (d,  $J$  = 2.7 Hz, 1H), 7.30 (d,  $J$  = 8.7 Hz, 2H), 5.91 (s, 1H), 3.37 (s, 3H), 2.06 (s, 3H).  $^{13}\text{C}$  NMR (101 MHz, DMSO- $d_6$ )  $\delta$  169.01, 157.02, 151.44, 147.87, 139.76, 137.59, 128.18, 120.06, 117.90, 113.07, 38.61, 24.51. HR-MS  $m/z$ : Calcd.  $\text{C}_{14}\text{H}_{14}\text{N}_3\text{O}_5$   $[\text{M}+\text{H}]^+$ : 304.0928; Found: 304.0929.

#### 4.4.13. *N*-(2-Acetamidophenyl)-5-nitrofur-2-carboxamide (**5A**)

Prepared from **15A** following general synthetic procedure B. Yellow crystal; Yield 74%; m.p. 212–213 °C.  $^1\text{H}$  NMR (400 MHz, DMSO- $d_6$ )  $\delta$  10.16 (s, 1H), 9.73 (s, 1H), 7.83 (d,  $J$  = 3.7 Hz, 1H), 7.60–7.56 (m, 3H), 7.27–7.20 (m, 2H), 2.10 (s, 3H).  $^{13}\text{C}$  NMR (101 MHz, DMSO- $d_6$ )  $\delta$  169.66, 155.28, 152.01, 148.57, 132.47, 129.03, 126.66, 125.28, 124.85, 116.89, 114.01, 23.99. HR-MS  $m/z$ : Calcd.  $\text{C}_{13}\text{H}_{12}\text{N}_3\text{O}_5$   $[\text{M}+\text{H}]^+$ : 290.0772; Found: 290.0770.

#### 4.4.14. *N*-(3-Acetamidophenyl)-5-nitrofur-2-carboxamide (**5B**)

Prepared from **15B** following general synthetic procedure B. Yellow solid; Yield 77%; m.p. 212–214 °C.  $^1\text{H}$  NMR (400 MHz, DMSO- $d_6$ )  $\delta$  10.63 (s, 1H), 10.03 (s, 1H), 8.09 (s, 1H), 7.82 (d,  $J$  = 3.9 Hz, 1H), 7.67 (d,  $J$  = 3.9 Hz, 1H), 7.44 (d,  $J$  = 7.8 Hz, 1H), 7.35–7.27 (m, 2H), 2.06 (s, 3H).  $^{13}\text{C}$  NMR (101 MHz, DMSO- $d_6$ )  $\delta$  168.87, 155.05, 152.27, 148.41, 140.15, 138.57, 129.39, 116.95, 115.93, 115.76, 113.89, 111.87, 24.52. HR-MS  $m/z$ : Calcd.  $\text{C}_{13}\text{H}_{12}\text{N}_3\text{O}_5$   $[\text{M}+\text{H}]^+$ : 290.0772; Found: 290.0769.

#### 4.4.15. *N*-(4-Methylphenyl)-5-nitrofur-2-carboxamide (**5C**)

Prepared from **15C** following general synthetic procedure B. Yellow solid; Yield 68%; m.p. 161–162 °C.  $^1\text{H}$  NMR (400 MHz,  $\text{CDCl}_3$ )  $\delta$  8.15 (s, 1H), 7.55 (d,  $J$  = 8.3 Hz, 2H), 7.41 (d,  $J$  = 3.8 Hz, 1H), 7.36 (d,  $J$  = 3.8 Hz, 1H), 7.20 (d,  $J$  = 8.3 Hz, 2H), 2.35 (s, 3H).  $^{13}\text{C}$  NMR (101 MHz,  $\text{CDCl}_3$ )  $\delta$  153.84, 148.01, 135.41, 133.76, 129.78, 120.42, 116.60, 112.68, 20.96. HR-MS  $m/z$ : Calcd.  $\text{C}_{12}\text{H}_{11}\text{N}_2\text{O}_4$   $[\text{M}+\text{H}]^+$ : 247.0713; Found: 247.0712.

#### 4.4.16. *N*-(4-Methoxyphenyl)-5-nitrofur-2-carboxamide (**5D**)

Prepared from **15D** following general synthetic procedure B. Yellow solid; Yield 72%; m.p. 185–187 °C.  $^1\text{H}$  NMR (400 MHz, DMSO- $d_6$ )  $\delta$  10.53 (s, 1H), 7.82 (d,  $J$  = 3.8 Hz, 1H), 7.65 (d,  $J$  = 8.8 Hz, 2H), 7.61 (d,  $J$  = 3.8 Hz, 1H), 6.96 (d,  $J$  = 8.8 Hz, 2H), 3.76 (s, 3H).  $^{13}\text{C}$  NMR (101 MHz, DMSO- $d_6$ )  $\delta$  156.61, 154.71, 152.14, 148.85, 131.21, 122.78, 116.63, 114.40, 113.98, 55.67. HR-MS  $m/z$ : Calcd.  $\text{C}_{12}\text{H}_{11}\text{N}_2\text{O}_5$   $[\text{M}+\text{H}]^+$ : 263.0663; Found: 263.0657.

#### 4.4.17. *N*-(4-Hydroxyphenyl)-5-nitrofur-2-carboxamide (**5E**)

Prepared from **15E** following general synthetic procedure B. Yellow solid; Yield 86%; m.p. 247–249 °C.  $^1\text{H}$  NMR (400 MHz, DMSO- $d_6$ )  $\delta$  10.42 (s, 1H), 9.39 (s, 1H), 7.80 (d,  $J$  = 3.9 Hz, 1H), 7.58 (d,  $J$  = 3.9 Hz, 1H), 7.50 (d,  $J$  = 8.8 Hz, 2H), 6.77 (d,  $J$  = 8.8 Hz, 2H).  $^{13}\text{C}$  NMR (101 MHz, DMSO- $d_6$ )  $\delta$  154.89, 154.59, 152.10, 148.82, 129.67, 123.03, 116.42, 115.64, 113.97. HR-MS  $m/z$ : Calcd.  $\text{C}_{11}\text{H}_9\text{N}_2\text{O}_5$   $[\text{M}+\text{H}]^+$ : 249.0506; Found: 249.0506.

#### 4.4.18. *N*-(4-Fluorophenyl)-5-nitrofur-2-carboxamide (**5F**)

Prepared from **15F** following general synthetic procedure B. Yellow solid; Yield 56%; m.p. 173–174 °C.  $^1\text{H}$  NMR (400 MHz,  $\text{CDCl}_3$ )  $\delta$  8.18 (s, 1H), 7.66–7.63 (m, 2H), 7.42 (d,  $J$  = 3.8 Hz, 1H), 7.38 (d,  $J$  = 3.8 Hz, 1H), 7.10 (t,  $J$  = 8.6 Hz, 2H).  $^{13}\text{C}$  NMR (101 MHz,  $\text{CDCl}_3$ )  $\delta$  160.08 (d,  $J$  = 246.5 Hz), 153.93, 147.65, 132.29, 122.31 (d,  $J$  = 8.1 Hz), 116.87, 116.07 (d,  $J$  = 22.8 Hz), 112.64. HR-MS  $m/z$ : Calcd.  $\text{C}_{11}\text{H}_8\text{FN}_2\text{O}_4$   $[\text{M}+\text{H}]^+$ : 251.0463; Found: 251.0461.

#### 4.4.19. *N*-(4-Chlorophenyl)-5-nitrofur-2-carboxamide (**5G**)

Prepared from **15G** following general synthetic procedure B. Yellow solid; Yield 80%; m.p. 179–180 °C.  $^1\text{H}$  NMR (400 MHz, DMSO- $d_6$ )  $\delta$  10.76 (s, 1H), 7.83 (d,  $J$  = 3.7 Hz, 1H), 7.78 (d,  $J$  = 8.6 Hz, 2H), 7.64 (d,  $J$  = 3.7 Hz, 1H), 7.45 (d,  $J$  = 8.6 Hz, 2H).  $^{13}\text{C}$  NMR (101 MHz, DMSO- $d_6$ )  $\delta$  155.09, 152.26, 148.11, 137.26, 129.22, 128.70, 122.67, 117.24, 113.93. HR-MS  $m/z$ : Calcd.  $\text{C}_{11}\text{H}_8\text{ClN}_2\text{O}_4$   $[\text{M}+\text{H}]^+$ : 267.0167; Found: 267.0167.

#### 4.4.20. *N*-(4-Cyanophenyl)-5-nitrofur-2-carboxamide (**5H**)

Prepared from **15H** following general synthetic procedure B. Yellow solid; Yield 75%; m.p. 229–231 °C.  $^1\text{H}$  NMR (400 MHz, DMSO- $d_6$ )  $\delta$  10.99 (s, 1H), 7.96 (d,  $J$  = 8.8 Hz, 2H), 7.87 (d,  $J$  = 8.8 Hz, 2H), 7.83 (d,  $J$  = 4.0 Hz, 1H), 7.70 (d,  $J$  = 4.0 Hz, 1H).  $^{13}\text{C}$  NMR (101 MHz, DMSO- $d_6$ )  $\delta$  155.47, 152.39, 147.68, 142.64, 133.74, 121.07, 119.31, 117.84, 113.88, 106.76.

#### 4.4.21. *N*-(4-Acetylphenyl)-5-nitrofur-2-carboxamide (**5I**)

Prepared from **15I** following general synthetic procedure B. Yellow solid; Yield 81%; m.p. 233–234 °C.  $^1\text{H}$  NMR (400 MHz, DMSO- $d_6$ )  $\delta$  10.91 (s, 1H), 7.99 (d,  $J$  = 8.0 Hz, 2H), 7.90 (d,  $J$  = 8.0 Hz, 2H), 7.82 (d,  $J$  = 2.4 Hz, 1H), 7.69 (d,  $J$  = 2.4 Hz, 1H), 2.55 (s, 3H).  $^{13}\text{C}$  NMR

(101 MHz, DMSO- $d_6$ )  $\delta$  197.13, 155.33, 152.36, 147.92, 142.68, 133.14, 129.84, 120.31, 117.57, 113.90, 26.98.

#### 4.4.22. Ethyl 4-(5-nitrofuran-2-carboxamido)benzoate (**5J**)

Prepared from **15J** following general synthetic procedure B. Yellow solid; Yield 77%; m.p. 221–223 °C.  $^1\text{H}$  NMR (400 MHz, DMSO- $d_6$ )  $\delta$  10.92 (s, 1H), 7.99 (d,  $J$  = 8.8 Hz, 2H), 7.91 (d,  $J$  = 8.8 Hz, 2H), 7.84 (d,  $J$  = 3.9 Hz, 1H), 7.70 (d,  $J$  = 3.9 Hz, 1H), 4.31 (q,  $J$  = 7.2 Hz, 2H), 1.33 (t,  $J$  = 7.2 Hz, 3H).  $^{13}\text{C}$  NMR (101 MHz, DMSO- $d_6$ )  $\delta$  165.67, 155.31, 152.36, 147.89, 142.72, 130.64, 125.84, 120.41, 117.55, 113.89, 61.05, 14.66. HR-MS  $m/z$ : Calcd.  $\text{C}_{14}\text{H}_{13}\text{N}_2\text{O}_6$   $[\text{M}+\text{H}]^+$ : 305.0768; Found: 305.0765.

#### 4.4.23. *N*-(4-Carbamoylphenyl)-5-nitrofuran-2-carboxamide (**5K**)

Prepared from **15K** following general synthetic procedure B. Yellow solid; Yield 87%; m.p. 297 °C (decomposed).  $^1\text{H}$  NMR (400 MHz, DMSO- $d_6$ )  $\delta$  10.85 (s, 1H), 7.96–7.91 (m, 3H), 7.85–7.82 (m, 3H), 7.72–7.70 (m, 1H), 7.37 (s, 1H).  $^{13}\text{C}$  NMR (101 MHz, DMSO- $d_6$ )  $\delta$  167.71, 155.21, 152.31, 148.93, 130.46, 128.81, 120.20, 117.37, 113.92. HR-MS  $m/z$ : Calcd.  $\text{C}_{12}\text{H}_{10}\text{N}_3\text{O}_5$   $[\text{M}+\text{H}]^+$ : 276.0615; Found: 276.0613.

#### 4.4.24. *N*-(4-(Dimethylamino)phenyl)-5-nitrofuran-2-carboxamide (**5L**)

Prepared from **15L** following general synthetic procedure B. Brown solid; Yield 63%; m.p. 202–205 °C.  $^1\text{H}$  NMR (400 MHz,  $\text{CDCl}_3$ )  $\delta$  8.09 (s, 1H), 7.52 (d,  $J$  = 8.8 Hz, 2H), 7.40 (d,  $J$  = 3.6 Hz, 1H), 7.34 (d,  $J$  = 3.6 Hz, 1H), 6.74 (d,  $J$  = 8.8 Hz, 2H), 2.96 (s, 6H).  $^{13}\text{C}$  NMR (101 MHz,  $\text{CDCl}_3$ )  $\delta$  153.58, 148.61, 148.45, 125.77, 122.02, 121.91, 116.19, 112.80, 112.73, 40.68. HR-MS  $m/z$ : Calcd.  $\text{C}_{13}\text{H}_{13}\text{N}_3\text{O}_4$   $[\text{M}+\text{H}]^+$ : 276.0979; Found: 276.0975.

#### 4.4.25. *N*-(4-Morpholinophenyl)-5-nitrofuran-2-carboxamide (**5M**)

Prepared from **15M** following general synthetic procedure B. Brown solid; Yield 45%; m.p. 208–209 °C.  $^1\text{H}$  NMR (400 MHz,  $\text{CDCl}_3$ )  $\delta$  8.11 (s, 1H), 7.58 (d,  $J$  = 8.4 Hz, 2H), 7.41 (s, 1H), 7.36 (s, 1H), 6.94 (d,  $J$  = 8.4 Hz, 2H), 3.87 (s, 4H), 3.17 (s, 4H).  $^{13}\text{C}$  NMR (101 MHz,  $\text{CDCl}_3$ )  $\delta$  153.69, 151.25, 149.06, 148.11, 128.70, 121.74, 116.49, 116.08, 112.81, 66.84, 49.32. HR-MS  $m/z$ : Calcd.  $\text{C}_{15}\text{H}_{16}\text{N}_3\text{O}_5$   $[\text{M}+\text{H}]^+$ : 318.1085; Found: 318.1083.

#### 4.4.26. *N*-(4-(4-Ethylpiperazin-1-yl)phenyl)-5-nitrofuran-2-carboxamide (**5N**)

Prepared from **15N** following general synthetic procedure B. Brown solid; Yield 71%; m.p. 185–186 °C.  $^1\text{H}$  NMR (400 MHz,  $\text{CDCl}_3$ )  $\delta$  8.10 (s, 1H), 7.55 (d,  $J$  = 8.4 Hz, 2H), 7.41 (s, 1H), 7.35 (s, 1H), 6.95 (d,  $J$  = 8.4 Hz, 2H), 3.23 (s, 4H), 2.62 (s, 4H), 2.49 (q,  $J$  = 7.0 Hz, 2H), 1.14 (t,  $J$  = 7.0 Hz, 3H).  $^{13}\text{C}$  NMR (101 MHz,  $\text{CDCl}_3$ )  $\delta$  153.73, 151.21, 149.10, 148.24, 128.38, 121.75, 116.43, 116.28, 112.86, 52.76, 52.38, 49.10, 12.05. HR-MS  $m/z$ : Calcd.  $\text{C}_{17}\text{H}_{21}\text{N}_4\text{O}_4$   $[\text{M}+\text{H}]^+$ : 345.1557; Found: 345.1553.

#### 4.5. General synthetic procedure C

Amines (**14B**–**14G**, 1.0 mmol) and DIEA (1.5 mmol, 194 mg) in dichloroethane (5 mL) were cooled to 0 °C, and then **7H** (1.0 mmol, 175 mg) in dichloroethane (2 mL) was dropped to the suspension. The reaction mixture was stirred at 65 °C for 3 h.

After cooled to r.t., the reaction mixture was concentrated and diluted with water (15 mL) and EtOAc (15 mL). The two layers were separated and the aqueous layer was extracted with EtOAc (15 mL  $\times$  2). The combined organic layer was washed successively with saturated  $\text{NaHCO}_3$  solution, 10% citric acid and brine, dried over anhydrous  $\text{Na}_2\text{SO}_4$ , filtered and concentrated. The residue was purified by column chromatography (silica gel, petroleum ether/ethyl acetate = 5:1, v/v) to afford the pure products.

#### 4.5.1. 5-Nitro-*N*-(pyridin-2-yl)furan-2-carboxamide (**2B**)

Prepared from **14B** following general synthetic procedure C. Yellow solid; Yield 46%; m.p. 189–190 °C.  $^1\text{H}$  NMR (400 MHz,  $\text{CDCl}_3$ )  $\delta$  8.94 (s, 1H), 8.38 (d,  $J$  = 4.6 Hz, 1H), 8.29 (d,  $J$  = 8.4 Hz, 1H), 7.79 (t,  $J$  = 7.8 Hz, 1H), 7.42 (s, 2H), 7.15 (t,  $J$  = 6.0 Hz, 1H).  $^{13}\text{C}$  NMR (101 MHz,  $\text{CDCl}_3$ )  $\delta$  154.15, 150.10, 148.30, 147.23, 138.64, 120.90, 117.22, 114.49, 112.42. HR-MS  $m/z$ : Calcd.  $\text{C}_{10}\text{H}_8\text{N}_3\text{O}_4$   $[\text{M}+\text{H}]^+$ : 234.0509; Found: 234.0507.

#### 4.5.2. 5-Nitro-*N*-(pyridin-3-yl)furan-2-carboxamide (**2C**)

Prepared from **14C** following general synthetic procedure C. Yellow solid; Yield 63%; m.p. 205–208 °C.  $^1\text{H}$  NMR (400 MHz, DMSO- $d_6$ )  $\delta$  10.87 (s, 1H), 8.91 (s, 1H), 8.37 (d,  $J$  = 3.8 Hz, 1H), 8.15 (d,  $J$  = 8.2 Hz, 1H), 7.84 (d,  $J$  = 3.2 Hz, 1H), 7.66 (d,  $J$  = 3.2 Hz, 1H), 7.44 (dd,  $J$  = 8.2, 3.8 Hz, 1H).  $^{13}\text{C}$  NMR (101 MHz, DMSO- $d_6$ )  $\delta$  155.45, 152.30, 147.89, 145.88, 142.69, 135.04, 128.33, 124.16, 117.50, 113.93. HR-MS  $m/z$ : Calcd.  $\text{C}_{10}\text{H}_8\text{N}_3\text{O}_4$   $[\text{M}+\text{H}]^+$ : 234.0509; Found: 234.0509.

#### 4.5.3. 5-Nitro-*N*-(pyridin-4-yl)furan-2-carboxamide (**2D**)

Prepared from **14D** following general synthetic procedure C. Yellow solid; Yield 45%; m.p. 230–232 °C.  $^1\text{H}$  NMR (400 MHz, DMSO- $d_6$ )  $\delta$  10.94 (s, 1H), 8.52 (d,  $J$  = 5.2 Hz, 2H), 7.83 (d,  $J$  = 3.2 Hz, 1H), 7.75 (d,  $J$  = 5.2 Hz, 2H), 7.70 (d,  $J$  = 3.2 Hz, 1H).  $^{13}\text{C}$  NMR (101 MHz, DMSO- $d_6$ )  $\delta$  155.78, 152.42, 150.96, 147.54, 145.26, 117.91, 114.72, 113.84. HR-MS  $m/z$ : Calcd.  $\text{C}_{10}\text{H}_8\text{N}_3\text{O}_4$   $[\text{M}+\text{H}]^+$ : 234.0509; Found: 234.0504.

#### 4.5.4. 5-Nitro-*N*-(pyrazin-2-yl)furan-2-carboxamide (**2E**)

Prepared from **14E** following general synthetic procedure C. Yellow solid; Yield 46%; m.p. 211–212 °C.  $^1\text{H}$  NMR (400 MHz, DMSO- $d_6$ )  $\delta$  11.60 (s, 1H), 9.38 (s, 1H), 8.53 (s, 1H), 8.48 (d,  $J$  = 2.4 Hz, 1H), 7.91 (d,  $J$  = 4.0 Hz, 1H), 7.83 (d,  $J$  = 4.0 Hz, 1H).  $^{13}\text{C}$  NMR (101 MHz, DMSO- $d_6$ )  $\delta$  155.59, 152.72, 148.63, 147.10, 143.27, 137.86, 118.16, 113.70. HR-MS  $m/z$ : Calcd.  $\text{C}_9\text{H}_6\text{N}_4\text{O}_4$   $[\text{M}+\text{H}]^+$ : 235.0462; Found: 235.0461.

#### 4.5.5. 5-Nitro-*N*-(pyrimidin-2-yl)furan-2-carboxamide (**2F**)

Prepared from **14F** following general synthetic procedure C. Yellow solid; Yield 32%; m.p. 207–208 °C.  $^1\text{H}$  NMR (400 MHz, DMSO- $d_6$ )  $\delta$  11.43 (s, 1H), 8.93–8.63 (m, 2H), 7.82 (d,  $J$  = 2.0 Hz, 2H), 7.32 (t,  $J$  = 4.8 Hz, 1H).  $^{13}\text{C}$  NMR (101 MHz, DMSO- $d_6$ )  $\delta$  159.11, 157.78, 154.77, 152.64, 147.71, 118.42, 117.86, 113.70. HR-MS  $m/z$ : Calcd.  $\text{C}_9\text{H}_6\text{N}_4\text{O}_4$   $[\text{M}+\text{H}]^+$ : 235.0462; Found: 235.0458.

#### 4.5.6. 5-Nitro-*N*-(pyridazin-3-yl)furan-2-carboxamide (**2G**)

Prepared from **14G** following general synthetic procedure C. Yellow solid; Yield 51%; m.p. 209–211 °C.  $^1\text{H}$  NMR (400 MHz, DMSO- $d_6$ )  $\delta$  11.91 (s, 1H), 9.07 (d,  $J$  = 4.2 Hz, 1H), 8.36 (d,  $J$  = 9.0 Hz, 1H), 7.95 (d,  $J$  = 3.2 Hz, 1H), 7.84 (d,  $J$  = 3.2 Hz, 1H), 7.80–7.77 (m, 1H).  $^{13}\text{C}$  NMR (101 MHz, DMSO- $d_6$ )  $\delta$  156.10, 155.61, 152.67, 149.67, 147.13, 129.17, 120.06, 118.10,

113.65. HR-MS  $m/z$ : Calcd.  $C_9H_7N_4O_4$   $[M+H]^+$ : 235.0462; Found: 235.0461.

#### 4.6. Animals

$C_{57}BL/6$  mice (body weight: 20–21 g, male) and adult male Sprague–Dawley (SD) rats (body weight: 190–210 g) were supplied by the Experimental Animal Center, Peking University (Beijing, China). UT-B knockout mice in a  $C_{57}BL/6$  genetic background were introduced from the University of California, San Francisco (UCSF, San Francisco, CA, USA)<sup>13</sup>. UT-A1 knockout mice in a  $C_{57}BL/6$  genetic background were generated by targeted gene disruption. All animal protocols were approved by the Ethics Committee of Peking University (Beijing, China).

#### 4.7. Blood samples

Human venous blood was taken from a healthy adult male volunteer, which was approved by the Ethics Committee of Peking University, (Beijing, China). Rat blood was collected from male SD rats (210–230 g) by orbital venous plexus puncture. Mouse blood was collected from male (20–21 g) wild-type or UT-B-null mice on a  $C_{57}BL/6$  genetic background by eyeball extirpating. Blood samples used for erythrocyte lysis assay and stopped-flow light scattering assay were anticoagulated by 0.5% heparin. Erythrocyte was acquired by centrifugation (TDZ5-WS, Changsha, China, 2000 r/min) after washed by PBS (0.01 mol/L, pH = 7.4) for three times. Then the erythrocyte was used for experiments in 12 h.

#### 4.8. Compounds

Compounds for preliminary screening were purchased (Selleck, Shanghai, China) or gifted from of Peking University School of Pharmaceutical Sciences (Beijing, China) and were dissolved in DMSO.

#### 4.9. Erythrocyte lysis assay for determining UT-B inhibition activity

The erythrocyte lysis assay was adopted after modified from a method described previously<sup>25</sup>. Erythrocyte was diluted to a hematocrit value of 2% (200  $\mu$ L erythrocyte diluted in 10 mL PBS) in PBS (0.01 mol/L, pH = 7.4, r.t.) containing 1.25 mol/L urea and 5.0 mmol/L glucose. Erythrocyte was incubated at r.t. for 2 h. Moving 100  $\mu$ L of the erythrocyte suspension to a 96-well microplate, then added 1  $\mu$ L testing compound (8, 2, 0.5, 0.12, 0.03 and 0.007 mmol/L dissolved in DMSO) to erythrocyte suspension and shook it up with microoscillator (QILINBEIER, Haimen, China) for 1 min. After 5 min of incubation, 20  $\mu$ L of the erythrocyte suspension was rapidly transferred to a 96-well black wall microplate that contained 180  $\mu$ L isotonic PBS (0.01 mol/L PBS without urea). Following quickly and sufficiently mixing (blow and suck with the pipettor for ten times), erythrocyte lysis was quantified by measuring absorbance at 710 nm wavelength with a plate reader (BioTek, Winooski, VT, USA) within 5 min. Each assay plate included negative no-lysis controls (1.25 mol/L urea + isotonic PBS with 1% DMSO) and positive full-lysis controls (distilled  $H_2O$  with 1% DMSO) that were mixed with vehicle-treated erythrocyte suspension.

The percentage of erythrocyte lysis in each test well was calculated using control values from the same plate as Eq. (1):

$$\text{Lysis}(\%) = (A_{\text{neg}} - A_{\text{test}}) / (A_{\text{neg}} - A_{\text{pos}}) \times 100 \quad (1)$$

where  $A_{\text{test}}$ ,  $A_{\text{neg}}$  and  $A_{\text{pos}}$  are the absorbance values from a test well, a negative no-lysis control well and a positive full-lysis control respectively.  $IC_{50}$ s are calculated by the software Graphpad Prism 5 with a log (inhibitor) vs. response analysis.

#### 4.10. Measurement of urea permeability in erythrocyte by stopped-flow light scattering

Erythrocyte was acquired from rat blood and suspended in PBS (0.01 mol/L, pH = 7.4, r.t.) to 0.5% (50  $\mu$ L erythrocyte diluted in 10 mL PBS). Then erythrocyte was incubated with targeted compounds for 5 min and quickly mixed with 500 mmol/L urea dissolved in PBS in an SX20 instrument (Applied Photophysics, Leatherhead, UK) with dead time of  $\sim 1.2$  ms as described previously<sup>53,54</sup>. The stopped-flow light scattering was measured as the time course of 90° scattered light intensity at 530 nm. Keep samples and PBS at 4 °C to reduce the influence of free diffusion. To test reversibility, compounds were added to erythrocyte for 5 min, then washed with PBS [1 mL erythrocyte was washed out by 10 mL PBS, and erythrocyte was acquired by 2000 r/min centrifugation (TDZ5-WS)] for 3 times before stopped-flow measurements. To determine inhibition on urea efflux, erythrocyte was incubated with 500 mmol/L urea dissolved in PBS for 2 h, then mixed with PBS without urea.

#### 4.11. Cytotoxicity assay

MDCK cells (passage numbers: 4–5) were cultured at 37 °C in a humidified 95% air/5%  $CO_2$  atmosphere in Dulbecco's modified Eagle's medium (DMEM, Gibco, Carlsbad, USA) supplemented with 10% fetal bovine serum (Hyclone, South Logan, UT, USA), 100 U/mL penicillin, and 100 mg/mL streptomycin. MDCK cells were cultured in a 96-well plate (5000 cells per well). When cells were grown to 50% confluence, synchronized by DMEM without fetal bovine serum for 12 h. Then cells were exposed to the compounds (**1H**, **5B** and **5K**) at 0, 15.6, 31.3, 62.5, 125 and 250  $\mu$ mol/L for 24 h. A cell counting kit-8 (Dojindo, Kumamoto, Japan) was used to measure cytotoxicity of compounds with different concentrations. The absorbance at 450 nm was measured 1–2 h after CCK-8 solution (10%, 100  $\mu$ L per well) was added to each well. Cytotoxicity was expressed as cell viability rate. The cell viability rate was calculated using control values from the same plate as Eq. (2):

$$\text{Lysis}(\%) = (OD_{\text{test}} - OD_{\text{blank}}) / (OD_{\text{control}} - OD_{\text{blank}}) \times 100 \quad (2)$$

where  $OD_{\text{test}}$ ,  $OD_{\text{blank}}$  and  $OD_{\text{control}}$  are the absorbance values from a test well, a blank control well and a solvent control well respectively.

#### 4.12. Assay of UT-A1-mediated and UT-B-mediated urea permeability

MDCK cells steadily expressing the UT-A1 or UT-B were used. The mRNA level of UT-A1 and UT-B was measured in our previous research<sup>37</sup>. Measurement of urea flux was as described previously<sup>36</sup>. MDCK cells ( $2 \times 10^5$  cells/cm<sup>2</sup>) that stably expressed rat UT-A1 were grown on 12 mm collagen-coated Costar Transwell inserts (0.4  $\mu$ m pore size; Corning, NY, USA)



for 4 days at 37 °C in the presence of 5% CO<sub>2</sub>. When cells in the apical side grew to become tight monolayer (transepithelial resistance 1 kΩ/cm<sup>2</sup>), PBS (pH = 7.4, containing 10 μmol/L forskolin) with **1H** or DMSO was added into top (0.25 mL) and bottom (1 mL) and cultures were incubated in the absence of urea for 30 min at 37 °C. As UT-B is located in the plasma membrane while UT-A1 is located in the cytoplasm, so forskolin was used to stimulate the transport of UT-A1 from cytoplasm to membrane to transport urea. Then, the solution in the bottom was replaced by PBS (pH = 7.4, containing 10 μmol/L forskolin, and containing **1H** or DMSO) with 15 mmol/L urea. The solution on the top (5 μL) was collected at 0, 1, 3, 5, 10, 15, 20, 30, 40, 50, and 60 min to test the urea concentration by QuantiChrom Urea Assay kit (BioAssay Systems, Hayward, CA, USA). The initial slope of urea concentration curve was calculated by absorbance values at 520 nm by Graphpad Prism 5. Inhibition of UT-A1-mediated urea permeability was calculated as Eq. (3):

$$\text{Inhibition(\%)} = \frac{(\text{DMSO}_{\text{initial slope}} - \text{1H}_{\text{initial slope}})}{(\text{DMSO}_{\text{initial slope}} - \text{Control}_{\text{initial slope}})} \times 100 \quad (3)$$

where  $\text{1H}_{\text{initial slope}}$  and  $\text{DMSO}_{\text{initial slope}}$  are initial slope values of cultures treated with **1H** or DMSO.  $\text{control}_{\text{initial slope}}$  is initial slope values of MDCK cells without UT expression.

The method to measure the UT-B-mediated urea permeability was the same as the method to measure the UT-A1-mediated urea transport except the PBS without forskolin because UT-B was highly expressed in the MDCK cell membrane.

The method to measure the IC<sub>50</sub> on rat UT-A1 was the same as the method to measure the UT-A1-mediated urea transport except the concentration of **1H** was 5, 1.25, 0.31, 0.08, 0.02, and 0.005 μmol/L. IC<sub>50</sub> was calculated by the software Graphpad Prism 5 with a log (inhibitor) vs. response analysis.

#### 4.13. Measurement of diuretic activity

Male wild-type mice, UT-B knockout mice (acquired by CRISPR/Cas9 gene-editing technique)<sup>13</sup>, UT-A1 knockout mice (acquired by CRISPR/Cas9 gene-editing technique)<sup>55</sup>, or SD rats were adapted in metabolic cages<sup>38</sup> (Ugo Basile, Comerio, VA, Italy) for 3 days. Water and food were provided *ad libitum*. Bladder was emptied by gentle abdominal massage and urine was collected by metabolic cages every 2 h. **1H** (10 mg/mL) in corn oil (Yuanye, Shanghai, China) was administered by subcutaneous injection or in carboxymethylcellulose sodium (CMC-Na, Sigma, St. Louis, MO, USA) was administered by gavage on mice or rats (100 mg/kg). Corn oil or CMC-Na was used as a vehicle control. Urine volume was measured by gravimetry, assuming a density of 1 g/mL. Urinary osmolality was measured by freezing point depression (Micro-osmometer; Fisker Associates, Norwood, MA, USA). Urea concentration was measured with the QuantiChrom urea assay kit (BioAssay Systems).

In long-term diuretic activity experiments, **1H** (10 mg/mL) dissolved in CMC-Na was administered to rats at a dose of 100 mg/kg (the first dose was double in order to reach an effective concentration faster) by gavage every 8 h. CMC-Na was used as a vehicle control. Urine was collected every 24 h by metabolic cages. Body weight and water intake were measured every day. Two hours after the last administration, a blood sample was collected by heart puncture. Inner medulla and outer medulla tissue homogenates were obtained, and the supernatant after

centrifugation was assayed for solute concentration and osmolality. Urinary osmolality and urea concentration were measured as above. Serum Na<sup>+</sup>, K<sup>+</sup>, Cl<sup>-</sup>, glucose, cholesterol, triglyceride, high-density lipoprotein, and low-density lipoprotein were measured in a clinical chemistry laboratory. Serum creatinine was measured through specific reagent kits (NJJC Bio, Nanjing, China).

#### 4.14. Measurement of GFR

We measure the GFR in mice using an optical device (Biostimech, Hong Kong, China) and the exogenous renal marker fluorescein isothiocyanate (FITC)-sinistrin<sup>56,57</sup>. After **1H** intra-gastric administration every 8 h for 7 days, wild-type mice were anesthetized by 3% isoflurane and then remove the fur by depilatory paste from the flank of the back. Fixation of the device on the animal, then inject through tail vein the FITC-sinistrin stock solution (15 mg/mL) at a dose of 50 mg/kg. Mice were placed in a calm place to avoid being disturbed. The measurement was performed during at least 1 h.

#### 4.15. Histology

Kidney and liver were fixed with paraformaldehyde and embedded in paraffin. 5 μm paraffin sections were cut and stained with hematoxylin and eosin.

#### 4.16. Transport assay in Caco-2 cell monolayer

Caco-2 cells (passage numbers: 42–50) were obtained from the American Type Cell Culture (ATCC; HTB-37, Manassas, VA, USA). Caco-2 cells were maintained in the sterile cell culture flasks (Corning Life Science) at 37 °C cell culture incubators (Thermo, Waltham, MA, USA) with 5% CO<sub>2</sub>, and saturated humidity in MEM with 10% FBS for cell culture. Caco-2 cells were seeded at a density of 50,000 cells/cm<sup>2</sup> into the apical chamber of Transwell® system (0.0804 cm<sup>2</sup>, 1 μm pore PC insert, Corning Life Science).

The transport assay in Caco-2 cell monolayer was conducted as previous reported<sup>58</sup>. The Lucifer Yellow (LY) rejection assay was conducted to determine the cell monolayer integrity at the same duration of test compounds in the assay. The solutions added into apical and basolateral wells were 75 and 250 μL respectively. The final concentration of all test compounds was 2 μmol/L in transport buffer. The plates of Caco-2 were incubated for 120 min in CO<sub>2</sub> incubator at 37 °C, with 5% CO<sub>2</sub> at saturated humidity. The initial dosing solution was mixed with stop solution (acetonitrile containing 250 ng/mL tolbutamide as the internal standard) as the T<sub>0</sub> sample. After reaching the incubation time, 50 μL terminal samples were collected from the donor and receiver sides of each well, and mixed with 250 μL stop solution for LC–MS/MS analysis. The apparent permeability ( $P_{\text{app}}$ , cm/s), efflux ratio (ER) and recovery parameters were calculated for drug transport assay using Eqs. (4) and (5):

$$P_{\text{app}} = \frac{V_R}{\text{Area} \times \text{Time}} \times \frac{[\text{Drug}]_{\text{receiver}}}{[\text{Drug}]_{\text{initial,donor}}} = \frac{V_R}{\text{Area} \times \text{Time}} \times \frac{C_R}{C_0} \quad (4)$$

$$\text{ER} = \frac{P_{\text{app}}(\text{B to A})}{P_{\text{app}}(\text{A to B})} \quad (5)$$

where  $V_R$  is the solution volume in the receiver chamber; Area is the surface area for the insert membrane, *i.e.*, 0.0804 cm<sup>2</sup> for the area of the monolayer; Time is incubation time, expressed in s;  $C_0$  is the initial peak area ratio (PAR) of control compounds in the donor chamber.

The high permeability compound metoprolol (TargetMol, Boston, USA) and a P-gp substrate digoxin (Sigma–Aldrich, St. Louis, USA) were used as controls in the assay, and the inhibitor of multiple efflux transporters GF120918 was added to determine that whether **1H** is a substrate of efflux transporters.

#### 4.17. Rat pharmacokinetics

Male SD rats (7–9 weeks, 250–270 g) were purchased from Vital River (Beijing, China) and fed with standard food and water at a stable temperature ( $22 \pm 2$  °C) and humidity ( $55 \pm 5\%$ ) with a 12 h light–dark cycle. A 10.0 mg/mL **1H** suspension resolved in 0.5% CMC-Na was administrated at 100 mg/kg in oral routine. Blood samples (250 µL) were collected *via* tail vein puncture at 0.083, 0.25, 0.5, 1, 2, 4, 6, 8, 12, and 24 h in tubes with anticoagulant (K<sub>2</sub>EDTA), and the plasma samples were obtained by centrifugation at 4000 rpm (ThermoScientific, Shanghai, China) for 15 min. The plasma samples were spiked with 200 µL of 5 ng/mL terfenadine (internal standard, IS) in MeOH/acetonitrile (1:1, *v/v*), vortexed for 1 min and centrifuged at 4000 rpm (ThermoScientific) for 15 min. The supernatant was diluted 10-fold with MeOH/water (1:1, *v/v*, with 0.1% formic acid) for injection, and the injection volume was 6 µL. The calibration standards were prepared by spiking the working solution into untreated rat plasma at the final concentrations of 1–1000 ng/mL. The calibration curves were fitted with a linear regression model ( $r > 0.99$ ) weighted by  $1/(x \times x)$ . The oral bioavailability was calculated by  $(AUC_{p.o.} \times Dose_{i.v.}) / (AUC_{i.v.} \times Dose_{p.o.})$ .

#### 4.18. Sample analysis

Analysis of rat plasma was performed on a high-performance liquid chromatography–tandem mass spectrometry (HPLC–MS/MS) system consisting of an API 5500 Mass Spectrometer (AB Sciex, Foster City, CA, USA), Shimadzu LC-20AD and Shimadzu SIL-20 A C (Shimadzu, Japan). The MS acquisition was operated in the electrospray (ESI) positive mode. Chromatographic separation was performed on a Kinetex 2.6 µm C18 100 Å column, 50 mm × 3.00 mm (Phenomenex, Torrance, CA, USA) at r.t. using a mobile phase of 5 mmol/L NH<sub>4</sub>OAc supplemented with 0.05% (*v/v*) formic acid (solvent A) and acetonitrile supplemented with 0.1% (*v/v*) formic acid (solvent B). The gradient was performed with a total flow at 0.7 mL/min as follow: 0–0.40 min 5% (B), 0.40–2.20 min 5%–95% (B), 2.20–2.30 min 95% (B), 2.30–2.31 min 95%–5% (B), 2.31–3.00 min 5% (B). Quantification was achieved by multiple reaction monitoring to identify the analytes (**1H**) and IS (terfenadine). The retention times of **1H** and IS were 1.73 and 2.08 min, respectively. The declustering potential (DP) and collision energy (CE) were optimized as followed: DP: 61V CE: 29V for **1H**, DP: 66V CE: 50V for terfenadine. The selected mass transitions were  $m/z$  290.1 → 231.2 for **1H**,  $m/z$  472.4 → 436.4 for terfenadine, respectively. AB SCIEX Analyst® software (version 1.6.1) was used for data acquisition and analysis.

#### 4.19. Molecular docking

A homology model of human UT-B was generated using the SWISS MODEL online utility (<http://swissmodel.expasy.org>) in automated mode, using the sequence of the full human UT-B protein (accession code, CAB60834). **1H** was drawn in ChemDraw (CambridgeSoftware, Cambridge, MA, USA). The UT-B protein was prepared for docking using the Protein Preparation (maestro, Schrödinger), using the homology model of human UT-B. **1H** was prepared using the LigPrep (maestro, Schrödinger). Docking was performed using Ligand Docking.

#### 4.20. Data analysis

Statistical analysis was performed using Graphpad Prism 5 software. All of the quantitative data are expressed as means ± SEM. Statistical analysis was performed using Student's *t*-test, one-way ANOVA followed by Fisher's least significant difference analysis for multiple comparisons.  $P < 0.05$  was considered statistically significant.

#### Acknowledgments

This work was supported by National Natural Science Foundation of China (Grant Nos.81620108029, 81974083, and 81330074), and Beijing Natural Science Foundation grant 7172113 (China).

#### Author contributions

Shun Zhang, Yan Zhao, Runtao Li, Baoxue Yang designed experiments. Shun Zhang, Yan Zhao, Shuyuan Wang, Min Li, Yue Xu carried out experiments. Shun Zhang, Yan Zhao, Jianhua Ran, Xiaoqiang Geng, Jinzhao He, Jia Meng, Guangying Shao, Hong Zhou, Zemei Ge, Guangping Chen analyzed experimental results. The manuscript was written through contributions of all authors. All authors have given approval to the final version of the manuscript.

#### Conflicts of interest

The authors declare no competing financial interests.

#### Appendix A. Supporting information

Supporting data related to this article can be found at <https://doi.org/10.1016/j.apsb.2020.06.001>.

#### References

- Oh SW, Han SY. Loop diuretics in clinical practice. *Electrolyte Blood Press* 2015;13:17–21.
- Jolobe OM. Diuretic-induced hyponatraemia in elderly hypertensive women. *J Hum Hypertens* 2003;17:151.
- Campo C, Ruilope LM, Segura J, Rodicio JL, Garcia-Robles R, Garcia-Puig J. Hyperuricemia, low urine urate excretion and target organ damage in arterial hypertension. *Blood Pres* 2003;12:277–83.
- Li M, Zhang S, Yang B. Urea transporters identified as a novel diuretic drug target. *Curr Drug Targets* 2020;21:279–87.
- Verkman AS, Esteva-Font C, Cil O, Anderson MO, Li F, Li M, et al. Small-molecule inhibitors of urea transporters. *Subcell Biochem* 2014;73:165–77.
- Sands JM. Renal urea transporters. *Curr Opin Nephrol Hypertens* 2004;13:525–32.

7. Li X, Chen G, Yang B. Urea transporter physiology studied in knockout mice. *Front Physiol* 2012;**3**:217.
8. Fenton RA, Yang B. Urea transporter knockout mice and their renal phenotypes. *Subcell Biochem* 2014;**73**:137–52.
9. Lei T, Zhou L, Layton AT, Zhou H, Zhao X, Bankir L, et al. Role of thin descending limb urea transport in renal urea handling and the urine concentrating mechanism. *Am J Physiol Ren Physiol* 2011;**301**:F1251–9.
10. Shayakul C, Clemencon B, Hediger MA. The urea transporter family (SLC14): physiological, pathological and structural aspects. *Mol Aspect Med* 2013;**34**:313–22.
11. Smith CP. Mammalian urea transporters. *Exp Physiol* 2009;**94**:180–5.
12. Fenton RA, Cottingham CA, Stewart GS, Howorth A, Hewitt JA, Smith CP. Structure and characterization of the mouse UT-A gene (*Slc14a2*). *Am J Physiol Ren Physiol* 2002;**282**:F630–8.
13. Yang B, Bankir L, Gillespie A, Epstein CJ, Verkman AS. Urea-selective concentrating defect in transgenic mice lacking urea transporter UT-B. *J Biol Chem* 2002;**277**:10633–7.
14. Huang B, Wang H, Yang B. Water transport mediated by other membrane proteins. *Adv Exp Med Biol* 2017;**969**:251–61.
15. Sands JM. Urea transporter inhibitors: en route to new diuretics. *Chem Biol* 2013;**20**:1201–2.
16. Fenton RA. Urea transporters and renal function: lessons from knockout mice. *Curr Opin Nephrol Hypertens* 2008;**17**:513–8.
17. Sands JM. Critical role of urea in the urine-concentrating mechanism. *J Am Soc Nephrol* 2007;**18**:670–1.
18. Fenton RA. Essential role of vasopressin-regulated urea transport processes in the mammalian kidney. *Pflügers Archiv* 2009;**458**:169–77.
19. Jiang T, Li Y, Layton AT, Wang W, Sun Y, Li M, et al. Generation and phenotypic analysis of mice lacking all urea transporters. *Kidney Int* 2017;**91**:338–51.
20. Yang B, Verkman AS. Urea transporter UT3 functions as an efficient water channel. Direct evidence for a common water/urea pathway. *J Biol Chem* 1998;**273**:9369–72.
21. Klein JD, Sands JM. Urea transport and clinical potential of ureauretics. *Curr Opin Nephrol Hypertens* 2016;**25**:444–51.
22. Esteva-Font C, Anderson MO, Verkman AS. Urea transporter proteins as targets for small-molecule diuretics. *Nat Rev Nephrol* 2015;**11**:113–23.
23. Yang B, Bankir L. Urea and urine concentrating ability: new insights from studies in mice. *Am J Physiol Ren Physiol* 2005;**288**:F881–96.
24. Li M, Tou WI, Zhou H, Li F, Ren H, Chen CY, et al. Developing hypothetical inhibition mechanism of novel urea transporter B inhibitor. *Sci Rep* 2014;**4**:5775.
25. Levin MH, de la Fuente R, Verkman AS. Ureauretics: a small molecule screen yields nanomolar potency inhibitors of urea transporter UT-B. *Faseb J* 2007;**21**:551–63.
26. Yao C, Anderson MO, Zhang J, Yang B, Phuan PW, Verkman AS. Triazolothienopyrimidine inhibitors of urea transporter UT-B reduce urine concentration. *J Am Soc Nephrol* 2012;**23**:1210–20.
27. Cil O, Esteva-Font C, Tas ST, Su T, Lee S, Anderson MO, et al. Salt-sparing diuretic action of a water-soluble urea analog inhibitor of urea transporters UT-A and UT-B in rats. *Kidney Int* 2015;**88**:311–20.
28. Liu Y, Esteva-Font C, Yao C, Phuan PW, Verkman AS, Anderson MO. 1,1-Difluoroethyl-substituted triazolothienopyrimidines as inhibitors of a human urea transport protein (UT-B): new analogs and binding model. *Bioorg Med Chem Lett* 2013;**23**:3338–41.
29. Lee S, Esteva-Font C, Phuan PW, Anderson MO, Verkman AS. Discovery, synthesis and structure–activity analysis of symmetrical 2,7-disubstituted fluorenones as urea transporter inhibitors. *Medchem-comm* 2015;**6**:1278–84.
30. Esteva-Font C, Phuan PW, Lee S, Su T, Anderson MO, Verkman AS. Structure–activity analysis of thiourea analogs as inhibitors of UT-A and UT-B urea transporters. *Biochim Biophys Acta* 2015;**1848**:1075–80.
31. Li F, Lei T, Zhu J, Wang W, Sun Y, Chen J, et al. A novel small-molecule thienoquinolin urea transporter inhibitor acts as a potential diuretic. *Kidney Int* 2013;**83**:1076–86.
32. Zhao Y, Li M, Li B, Zhang S, Su A, Xing Y, et al. Discovery and optimization of thienopyridine derivatives as novel urea transporter inhibitors. *Eur J Med Chem* 2019;**172**:131–42.
33. Lee S, Cil O, Diez-Cecilia E, Anderson MO, Verkman AS. Nanomolar-potency 1,2,4-triazoloquinoxaline inhibitors of the kidney urea transporter UT-A1. *J Med Chem* 2018;**61**:3209–17.
34. Anderson MO, Zhang J, Liu Y, Yao C, Phuan PW, Verkman AS. Nanomolar potency and metabolically stable inhibitors of kidney urea transporter UT-B. *J Med Chem* 2012;**55**:5942–50.
35. Ran JH, Li M, Tou WI, Lei TL, Zhou H, Chen CY, et al. Phenylphthalazines as small-molecule inhibitors of urea transporter UT-B and their binding model. *Acta Pharmacol Sin* 2016;**37**:973–83.
36. Frohlich O, Klein JD, Smith PM, Sands JM, Gunn RB. Urea transport in MDCK cells that are stably transfected with UT-A1. *Am J Physiol Cell Physiol* 2004;**286**:C1264–70.
37. Li M, Zhao Y, Zhang S, Xu Y, Wang S, Li B, et al. A thienopyridine, CB-20, exerts diuretic activity by inhibiting urea transporters. *Acta Pharmacol Sin* 2020;**41**:65–72.
38. Ren H, Wang Y, Xing Y, Ran J, Liu M, Lei T, et al. Thienoquinolins exert diuresis by strongly inhibiting UT-A urea transporters. *Am J Physiol Ren Physiol* 2014;**307**:F1363–72.
39. Zhang ZY, Wang X, Liu D, Zhang H, Zhang Q, Lu YY, et al. Development and validation of an LC–MS/MS method for the determination of a novel thienoquinolin urea transporter inhibitor PU-48 in rat plasma and its application to a pharmacokinetic study. *Bio-med Chromatogr* 2018;**32**:e4157.
40. Zhang ZY, Zhang H, Liu D, Lu YY, Wang X, Li P, et al. Pharmacokinetics, tissue distribution and excretion of a novel diuretic (PU-48) in rats. *Pharmaceutics* 2018;**10**:124.
41. Carroll FI, Lewin AH, Mascarella SW, Seltzman HH, Reddy PA. Designer drugs: a medicinal chemistry perspective. *Ann N Y Acad Sci* 2012;**1248**:18–38.
42. Ehrh T, Brinkjost T, Koch O. Impact of binding site comparisons on medicinal chemistry and rational molecular design. *J Med Chem* 2016;**59**:4121–51.
43. Liang S, Zhang RY, Xi LY, Chen SY, Yu XQ. Sulfonation of five-membered heterocycles via an  $S_NAr$  reaction. *J Org Chem* 2013;**78**:11874–80.
44. Pallone TL, Turner MR, Edwards A, Jamison RL. Countercurrent exchange in the renal medulla. *Am J Physiol Regul Integr Comp Physiol* 2003;**284**:R1153–75.
45. Klein JD, Wang Y, Mistry A, LaRocque LM, Molina PA, Rogers RT, et al. Transgenic restoration of urea transporter A1 confers maximal urinary concentration in the absence of urea transporter A3. *J Am Soc Nephrol* 2016;**27**:1448–55.
46. Uchida S, Sohara E, Rai T, Ikawa M, Okabe M, Sasaki S. Impaired urea accumulation in the inner medulla of mice lacking the urea transporter UT-A2. *Mol Cell Biol* 2005;**25**:7357–63.
47. Fenton RA, Flynn A, Shodeinde A, Smith CP, Schnermann J, Knepper MA. Renal phenotype of UT-A urea transporter knockout mice. *J Am Soc Nephrol* 2005;**16**:1583–92.
48. Trinh-Trang-Tan MM, Lasbennes F, Gane P, Roudier N, Ripoché P, Cartron JP, et al. UT-B1 proteins in rat: tissue distribution and regulation by antidiuretic hormone in kidney. *Am J Physiol Ren Physiol* 2002;**283**:F912–22.
49. Dahan A, Miller JM, Hilfinger JM, Yamashita S, Yu LX, Lennernas H, et al. High-permeability criterion for BCS classification: segmental/pH dependent permeability considerations. *Mol Pharm* 2010;**7**:1827–34.
50. Liu GY, Zhou Y, Chen LY. Intestinal uptake of barley protein-based nanoparticles for  $\beta$ -carotene delivery. *Acta Pharm Sin B* 2019;**9**:87–96.
51. Elsbey R, Surry DD, Smith VN, Gray AJ. Validation and application of Caco-2 assays for the *in vitro* evaluation of development candidate drugs as substrates or inhibitors of P-glycoprotein to support regulatory submissions. *Xenobiotica* 2008;**38**:1140–64.
52. Li FF, Liu ZL, Sun HY, Li CM, Wang WY, Ye L, et al. PCC0208017, A novel small-molecule inhibitor of MARK3/MARK4, suppresses glioma progression *in vitro* and *in vivo*. *Acta Pharm Sin B* 2020;**10**:289–300.

53. Yang B, Verkman AS. Analysis of double knockout mice lacking aquaporin-1 and urea transporter UT-B. Evidence for UT-B-facilitated water transport in erythrocytes. *J Biol Chem* 2002;**277**:36782–6.
54. Mayrand RR, Levitt DG. Urea and ethylene glycol-facilitated transport systems in the human red cell membrane. Saturation, competition, and asymmetry. *J Gen Physiol* 1983;**81**:221–37.
55. Geng XQ, Zhang S, He JZ, Ma A, Li YJ, Li M, et al. Urea transporter UT-A1 plays a predominant role in urea dependent urine concentrating mechanism. *J Biol Chem* 2020;**295**:9893–900.
56. Herrera Perez Z, Weinfurter S, Gretz N. Transcutaneous assessment of renal function in conscious rodents. *JoVE* 2016;**109**:e53767.
57. Dorshow RB, Bugaj JE. Next tier *in vitro* and *in vivo* nonclinical studies further elucidating the safety and toxicity profile of MB-102, a novel fluorescent tracer agent for measurement of glomerular filtration rate. *Regul Toxicol Pharmacol* 2019;**107**:104417.
58. Skolnik S, Lin X, Wang J, Chen XH, He T, Zhang B. Towards prediction of *in vivo* intestinal absorption using a 96-well Caco-2 assay. *J Pharmacol Sci* 2010;**99**:3246–65.